FOREWORD

This volume is the thirtieth of the WADD Technical Report 61 - 72 series describing various phases of research and development on advanced graphite materials conducted by National Carbon Company, a Division of Union Carbide Corporation, under USAF Contract No. AF 33(616)-6915.

The work covered in this report was conducted from September, 1961 through December, 1962 at the Advanced Materials Laboratory and the Research Laboratory of National Carbon Company under the management of R. M. Bushong, Director of the Advanced Materials Project, J. C. Bowman, Director of Research, W. P. Eatherly, Assistant Director of Research, and R. C. Stroup, Manager of the Advanced Materials Laboratory.

The contract for this R&D program was initiated under Project No. 7350, "Refractory Inorganic Non-Metallic Materials," Task No. 735002, "Refractory Inorganic Non-Metallic Materials: Graphitic, Project No. 7381, "Materials Application," Task No. 738102, "Materials Processes," and Project No. 7-817, "Process Development for Graphite Materials." The work was administrated by the Air Force Materials Laboratory, Deputy Commander/Research and Engineering, Aeronautical Systems Division, Captain R. H. Wilson, L. J. Conlon, and W. P. Conrardy acting as Project Engineers.

The authors are pleased to acknowledge contributions by Drs. Rexer and Schissel, and Messrs. Beasley, Cannon, Null, and Rowe.

Other volumes in this WADD Technical Report 61-72 series are:

Volume I - Observations by Electron Microscopy of Dislocations in Graphite, by R. Sprague

Volume II - Applications of Anisotropic Elastic Continuum Theory to Dislocations in Graphite, by G. B. Spence

Volume III - Decoration of Dislocations and Low Angle Grain Boundaries in Graphite Single Crystals, by R. Bacon and R. Sprague

Volume IV - Adaptation of Radiographic Principles to the Quality Control of Graphite, by R. W. Wallouch

Volume V - Analysis of Creep and Recovery Curves for ATJ Graphite, by E. J. Seldin and R. N. Draper

Volume VI - Creep of Carbons and Graphites in Flexure at High Temperature, by E. J. Seldin

Volume VII - High Density Recrystallized Graphite by Hot-Forming, by E. A. Neel, A. A. Kellar, K. J. Zeitsch

Supplement - High Density Recrystallized Graphite by Hot-Forming, by G. L. Rowe and M. B. Carter

Volume VIII - Electron Spin Resonance in Polycrystalline Graphite, by L. S. Singer and G. Wagoner

Volume IX - Fabrication and Properties of Carbonized Cloth Composites, by W. C. Beasley and E. L. Piper

Volume X - Thermal Reactivity of Aromatic Hydrocarbons, by I. C. Lewis and T. Edstrom

Supplement - Thermal Reactivity of Aromatic Hydrocarbons, by I. C. Lewis and T. Edstrom

Volume XI - Characterization of Binders Used in the Fabrication of Graphite Bodies, by E. de Ruiter, A. Halleux, V. Sandor, H. Tschamler

Supplement - Characterization of Binders Used in the Fabrication of Graphite Bodies, by E. de Ruiter, J. F. M. Oth, V. Sandor and H. Tschamler

Volume XII - Development of an Improved Large Diameter Fine Grain Graphite for Aerospace Applications, by C. W. Waters and E. L. Piper

Supplement - Development of an Improved Large Diameter Fine Grain Graphite for Aerospace Applications, by R. L. Racicot and C. W. Waters

Volume XIII - Development of a Fine-Grain Isotropic Graphite for Structural and Substrate Applications, by R. A. Howard and E. L. Piper

Supplement - Development of a Fine-Grain Isotropic Graphite for Structural and Substrate Applications, by R. A. Howard and R. L. Racicot

Volume XIV - Study of High Temperature Tensile Properties of ZTA Grade Graphite, by R. M. Hale and W. M. Fassell, Jr.

Volume XV - Alumina-Condensed Furfuryl Alcohol Resins, by C. W. Boquist, E. R. Nielsen, H. J. O'Neil and R. E. Putcher

Volume XVI - An Electron Spin Resonance Study of Thermal Reactions of Organic Compounds, by L. S. Singer and I. C. Lewis

Volume XVII - Radiography of Carbon and Graphite, by T. C. Furnas, Jr. and M. R. Rosumny

Volume XVIII - High Temperature Tensile Creep of Graphite, by E. J. Seldin

Volume XIX - Thermal Stresses in Anisotropic Hollow Cylinders, by Tu-Lung Weng

Volume XX - The Electric and Magnetic Properties of Pyrolytic Graphite by G. Wagoner and B. H. Eckstein

Volume XXI - Arc Image Furnace Studies of Graphite, by M. R. Null and W. W. Lozier

Volume XXII - Photomicrographic Techniques for Carbon and Graphite, by G. L. Peters and H. D. Shade

Volume XXIII - A Method for Determining Young's Modulus of Graphite at Elevated Temperatures, by S. O. Johnson and R. B. Dull

Volume XXIV - The Thermal Expansion of Graphite in the c-Direction, by C. E. Lowell

Volume XXV - Lamellar Compounds of Nongraphitized Petroleum Cokes, by H. F. Volk

Volume XXVI - Physical Properties of Some Newly Developed Graphite Grades, by R. B. Dull

Volume XXVII - Carbonization Studies of Aromatic Hydrocarbons, by I. C. Lewis and T. Edstrom

Volume XXVIII - Polarographic Reduction of Polynuclear Aromatics, by I. C. Lewis, H. Beibecki, and S. L. Bushong

Volume XXIX - Evaluation of Graphite Materials in a Subscale Solid Propellant Rocket Motor, by D. C. Hiler and R. B. Dull

Supplement - Evaluation of Graphite Materials in a Subscale Solid Propellant Rocket Motor, by S. O. Johnson and R. B. Dull

ABSTRACT

This report describes certain graphite base composites capable of resisting oxidation by forming a protective coating from their oxidation products. When first exposed to oxidizing conditions, the additives or graphite-additive reactants oxidize and form a coating which protects the composite against further oxidation. Since these materials are homogeneous composites, they can be machined without destroying their oxidation resistant characteristics. The most effective additives investigated were combinations of ZrB_2, Si, B, Cb, and Th. All materials were prepared in a one step operation by hot pressing. The report describes the equipment required to fabricate graphite-refractory composites by hot pressing at temperatures up to 3100°C. Oxidation test methods employ indirect induction heating, resistance heating, arc image techniques, and electromagnetic levitation.

This technical documentary report has been reviewed and is approved.

W. G. RAMKE
Chief, Ceramics and Graphite Branch
Metals and Ceramics Division
Air Force Materials Laboratory

TABLE OF CONTENTS

LIST OF ILLUSTRATIONS

LIST OF ILLUSTRATIONS (Continued)

LIST OF ILLUSTRATIONS (Continued)

LIST OF ILLUSTRATIONS (Continued)

1. INTRODUCTION

Graphite is one of the most widely used high temperature materials because of its combination of refractoriness, thermal shock resistance, and machinability. Present-day applications, especially in the aerospace field, nevertheless, call for improvements of graphite with respect to oxidation resistance, strength, and hardness. Improvements of metals with respect to these properties have been accomplished by alloying and, in a similar manner, the purpose of this study has been to enhance the properties of graphite by the use of additives. The carbon content of the graphite-additive materials generally has exceeded 70 per cent by volume in order to preserve the basic features of graphite. This amount of carbon was considerably more than could be dissolved by the additives. Therefore, the resulting products to be discussed here are composites rather than alloys; nevertheless, alloying was evident in localized areas where molten phases occurred.

Manuscript released by the authors August 1963 for publication as an ASD Technical Documentary Report

2. GENERAL PROCESSING CHARACTERISTICS

All composites described in this report were manufactured in a one step operation by hot pressing. Graphite molds and carbon plungers were used exclusively, and heating was accomplished by induction. Final process temperatures ranged from 1800 to 3100°C, depending on the additives used, and molding pressures were between 2250 and 6350 lbs/in^2.

The starting materials are powdery blends consisting of coke or graphite, pitch, and the additives. Upon heating such blends under pressure, a significant primary compaction is achieved when the pitch melts between 100 and 200°C. This allows the solid particles of the system to arrange themselves in a dense pack. A carbon-bonded matrix is formed when the pitch converts to coke at about 600 to 800°C, after which no further densification takes place until this pitch coke, as well as any other coke in the system, reaches some degree of plasticity. The plastic range commences between 1700 and 1800°C and the degree of plasticity increases as the temperature rises. With the continued application of pressure, a secondary compaction takes place.

In general, the process is carried up to and beyond the point where a liquid phase appears in the system due to the melting of additives. The liquid phase is squeezed into the pores of the solid phase as the carbon matrix is plastically compressed and, upon cooling, an impervious body is formed. Varying amounts of the prevalent solid phase dissolve in the liquid phase in accordance with the equilibrium relations involved. Consequently, with the solubility limit being a function of temperature, processing conditions allow the adjustment of the degree of homogeneity within the composite.

Pitch in the starting material is a beneficial, but not absolutely necessary, ingredient. It allows dense packing by extensive liquefaction of the system which could be accomplished by molten refractory additives only if they were present in sizable volume. In forming a carbon matrix, the pitch not only provides the material with a respectable residual strength when exposed to temperatures at which a molten phase occurs but also prevents excessive escape of molten additives by trapping them in pores. The latter benefit applies to the material in eventual application as well as during processing.

3. FABRICATING EQUIPMENT

Presses with auxiliary heating equipment capable of producing the temperatures and pressures required for this study are not available commercially. This special equipment, consequently, had to be designed and constructed.

3.1. Development Equipment

Since a large number of compositions, in some cases containing expensive additives, would have to be investigated in this study, it was desirable to make the initial investigations with blanks of small size. Each blank, on the other hand, had to yield enough material for necessary oxidation tests and property measurements. As a compromise, it was decided to work with blanks 2 inches in diameter by 2 inches in length.

An overall view and the internal design of the press, mold, and heating equipment are illustrated in Figures 1 and 2. The mold and bottom plate were made of ATJ graphite whereas a strong, lampblack base material with a low creep rate at high temperature was used for the plunger and mold insert. The latter material is not commercially available and it will be referred to as grade CX for purposes of this report. The taper of the mold as shown in Figure 2, allows easy removal of the blank after processing.

The mold assembly rests on a column of CX material and is enclosed in fine lampblack powder. The latter in turn is confined by a tube of clay-bonded silicon carbide. An induction coil energized by a 50-kw, 3000-cycles-per-second motor generator set permits heating of the mold from room temperature to 3400°C within approximately one hour. The CX material supporting the mold is a sufficiently good thermal insulator to prevent high temperatures from reaching the bottom platen of the press. The upper platen, which is closer to the hot mold than the bottom platen, is equipped with a water-cooled head. Aluminum shielding protects the press frame from being heated by the electromagnetic field of the induction coil.

The force of the press can be increased at various uniform rates and automatically maintained at a constant value regardless of plunger travel. The maximum capacity of the press is 28 tons. Generally, less than one-half of this force is sufficient to process the 2-inch diameter blanks.

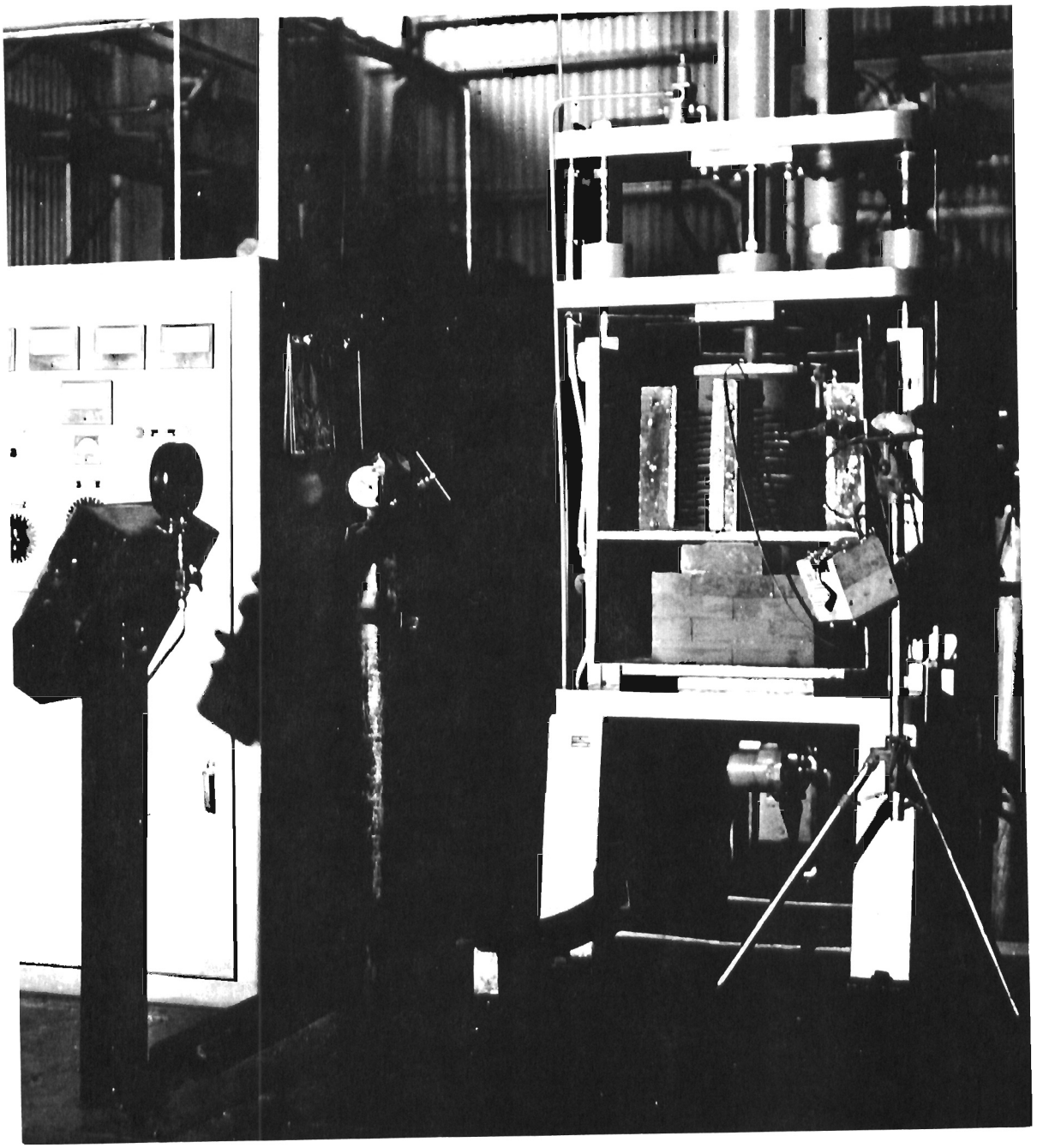

Figure 1. Small Hot Press for Development Purposes, Overall View

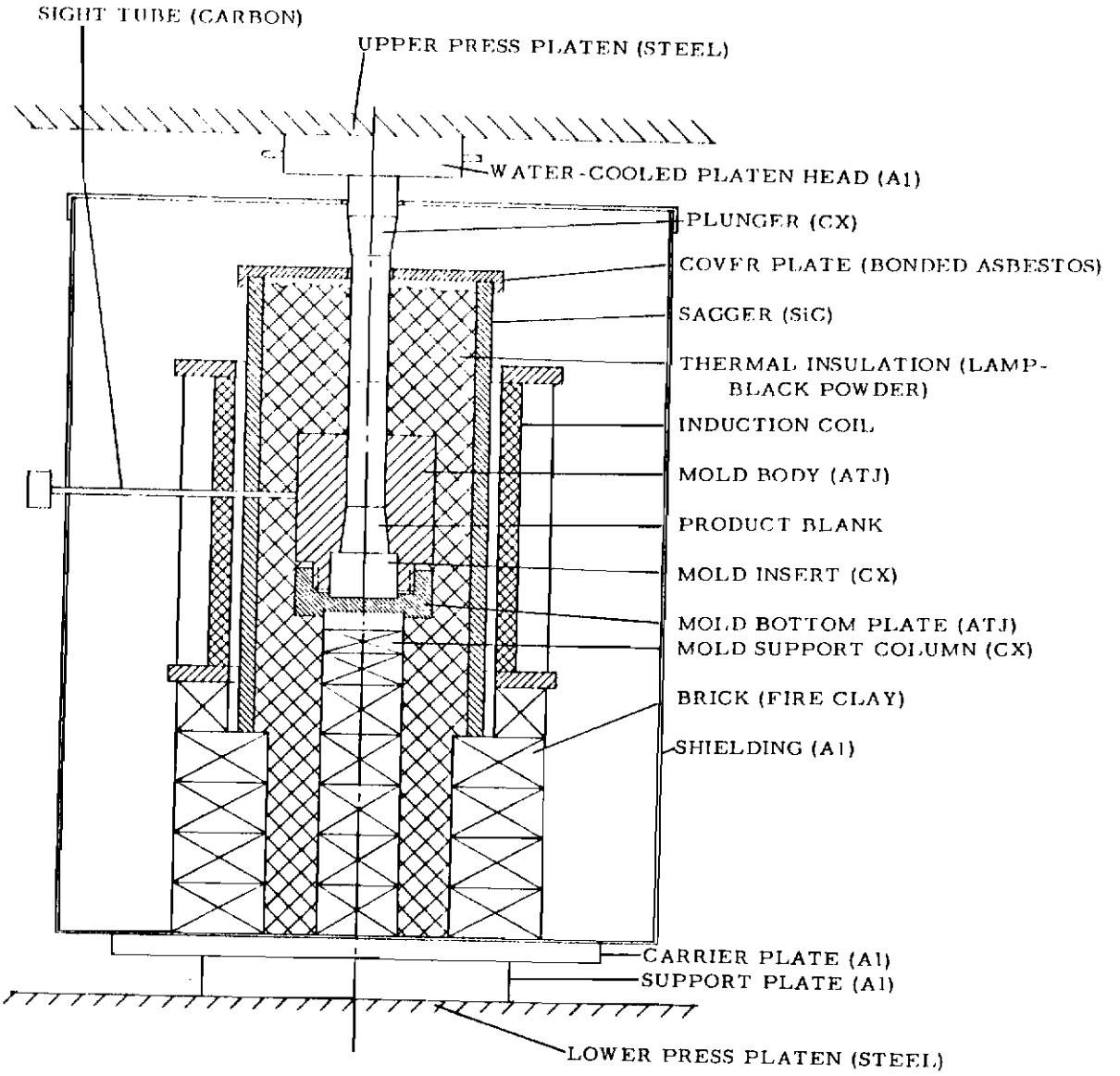

Figure 2. Small Hot Press for Development Purposes, Cross Section

3.2. Scale-Up Equipment

Composites were developed with promising properties and had to be made available in larger sizes in order to allow laboratory tests and larger scale evaluations not possible with the usual 2-inch diameter blanks. An enlarged version of the development equipment described above was constructed and used to fabricate composites of a 5-inch diameter size. A general view and a schematic drawing of this press and auxiliary equipment are illustrated in Figures 3 and 4. The press has a capacity of 300 tons and a movable bottom platen which facilitates loading operations.

The molding and heating equipment is similar to that used for development purposes. It should be pointed out that the silicon carbide tube containing the lampblack insulation is constructed of rings with tongue and groove joints, and that only the upper part of the lower mold-support column is made of CX material while the lower portion consists of a standard gas-baked carbon stock. The induction coil for this larger setup is energized by a 100-kw, 3000-cycles-per-second motor generator set.

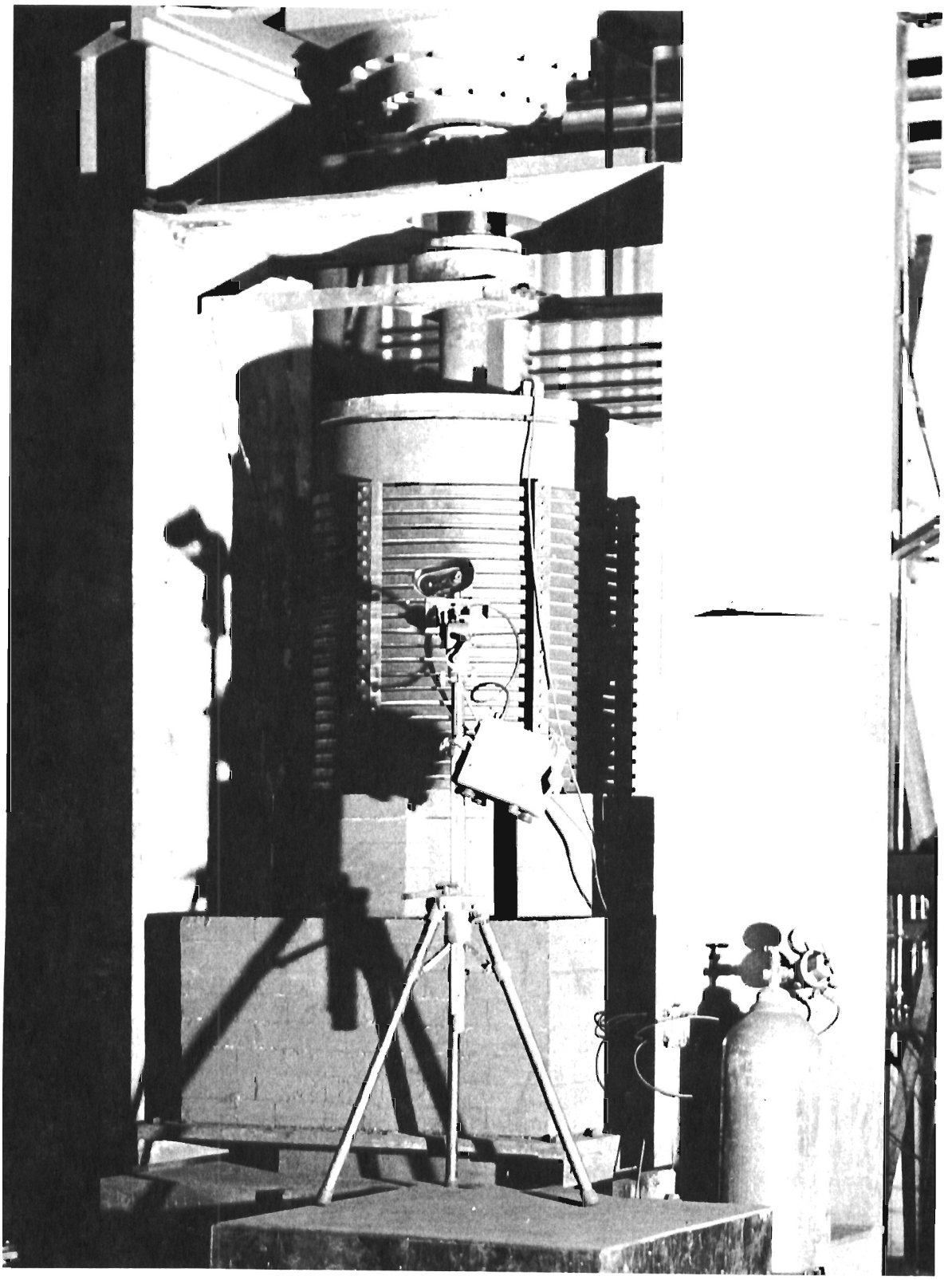

Figure 3. Large Hot Press for Scale-Up Purposes, Overall View

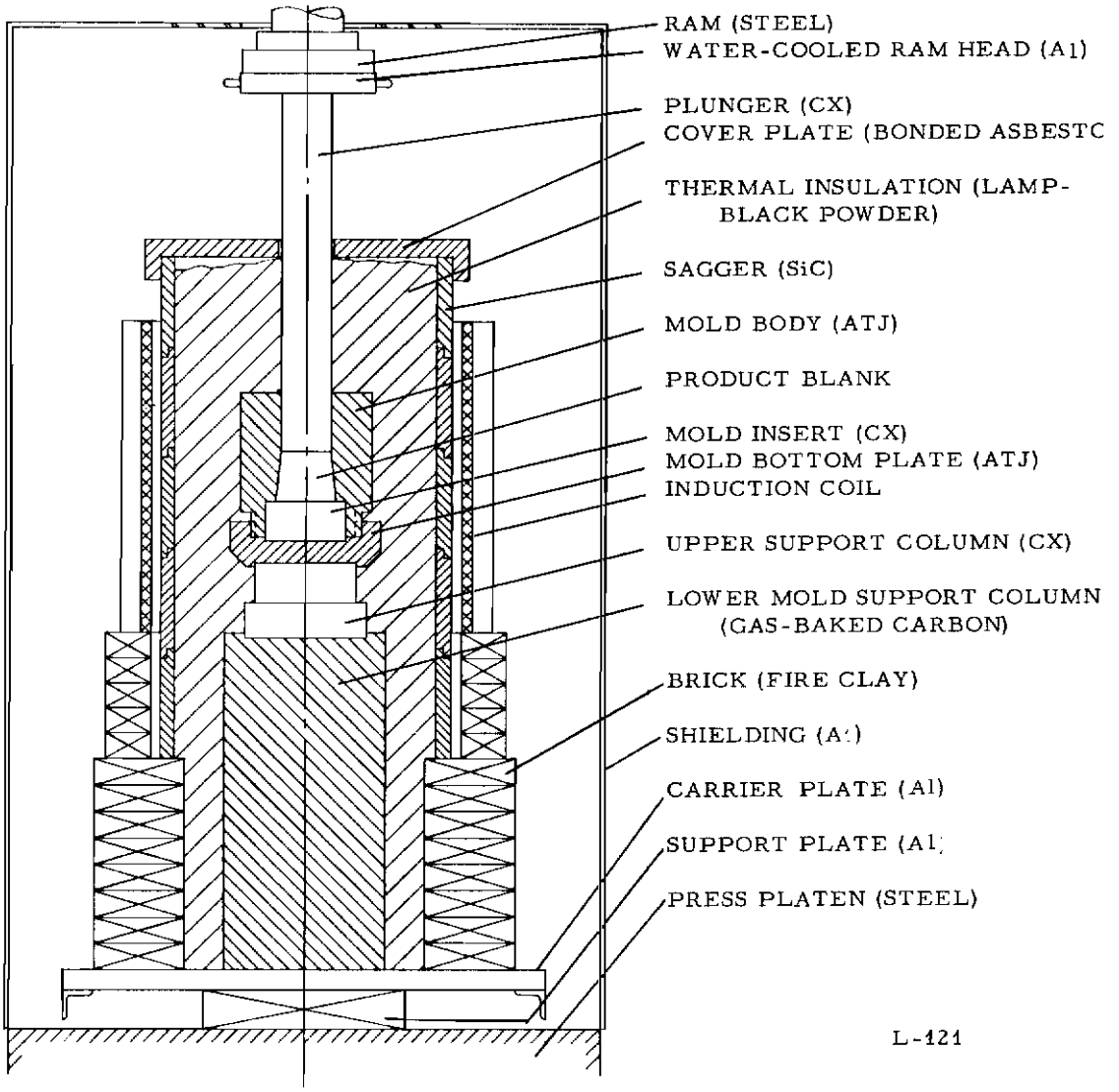

Figure 4. Large Hot Press for Scale-Up Purposes, Cross Section

4. TESTING EQUIPMENT

The graphite base composites were designed for high temperature applications and, therefore, their evaluation had to be carried out at elevated temperatures. While some of the techniques employed in this evaluation are commonly known in the graphite industry, others had to be newly developed specifically for this work. The apparatuses for measurements of oxidation resistance and strength fall in the latter category and will be discussed in detail while the common methods will be discussed only briefly with proper references.

4.1. Oxidation Measurements

Apparatuses for measuring oxidation, which are commercially available are limited to maximum temperatures of 1400°C. This temperature is too low for the intended investigations; therefore, high temperature devices had to be designed and constructed. Each of the resulting apparatuses was found to have some advantage so that no one design is outstandingly better than the others at all conditions.

4.1.1. Induction-Radiation Equipment

In available oxidation apparatuses, the test specimen is suspended with a platinum wire in a brick furnace which is heated by resistance elements. The bricks as well as the resistance elements limit the temperature to a range of 1200 and 1400°C, depending on the materials employed. The furnace is generally open to convective air flow without regard to flow rates. Oxidation measurements are carried out continuously by recording the weight change of the suspended sample with a special balance. The latter is an analytical balance equipped with electrical weight compensation. The current necessary to compensate a certain weight change is amplified and recorded in a calibrated manner.

The outstanding feature of this method is the fact that it is capable of providing a continuous and extremely accurate record of the sample behavior as a function of time and temperature. It was, therefore, considered worthwhile to extend the range of this technique by using it in conjunction with a furnace capable of providing temperatures in excess of those commonly available. An overall view of the resulting apparatus is shown in Figure 5 while Figure 6 presents a detailed cross section. The furnace chamber and sample are heated by radiation from a graphite susceptor energized by electromagnetic induction. The furnace chamber consists of an impervious alumina pipe which prevents oxygen from reaching the graphite susceptor. The latter constitutes the middle part in a column of graphite rings which keep carbon from touching and chemically destroying the hot alumina. The chamber head plate and the nozzle carrier ring are made of siliconized graphite since they are the only hot carbon parts exposed to oxygen.

The temperature of the sample is measured through a hole in the bottom plate of the furnace chamber by means of an optical pyrometer. A controlled amount of dried and purified air is fed to the chamber also through the hole in the bottom plate.

The platinum wire limits the temperature range of this setup to approximately 1700°C. Attempts to reach higher temperatures by replacing the platinum wire with rhodium wire or beryllia rods were un-

successful because both materials alloyed with the test specimen and disintegrated rapidly.

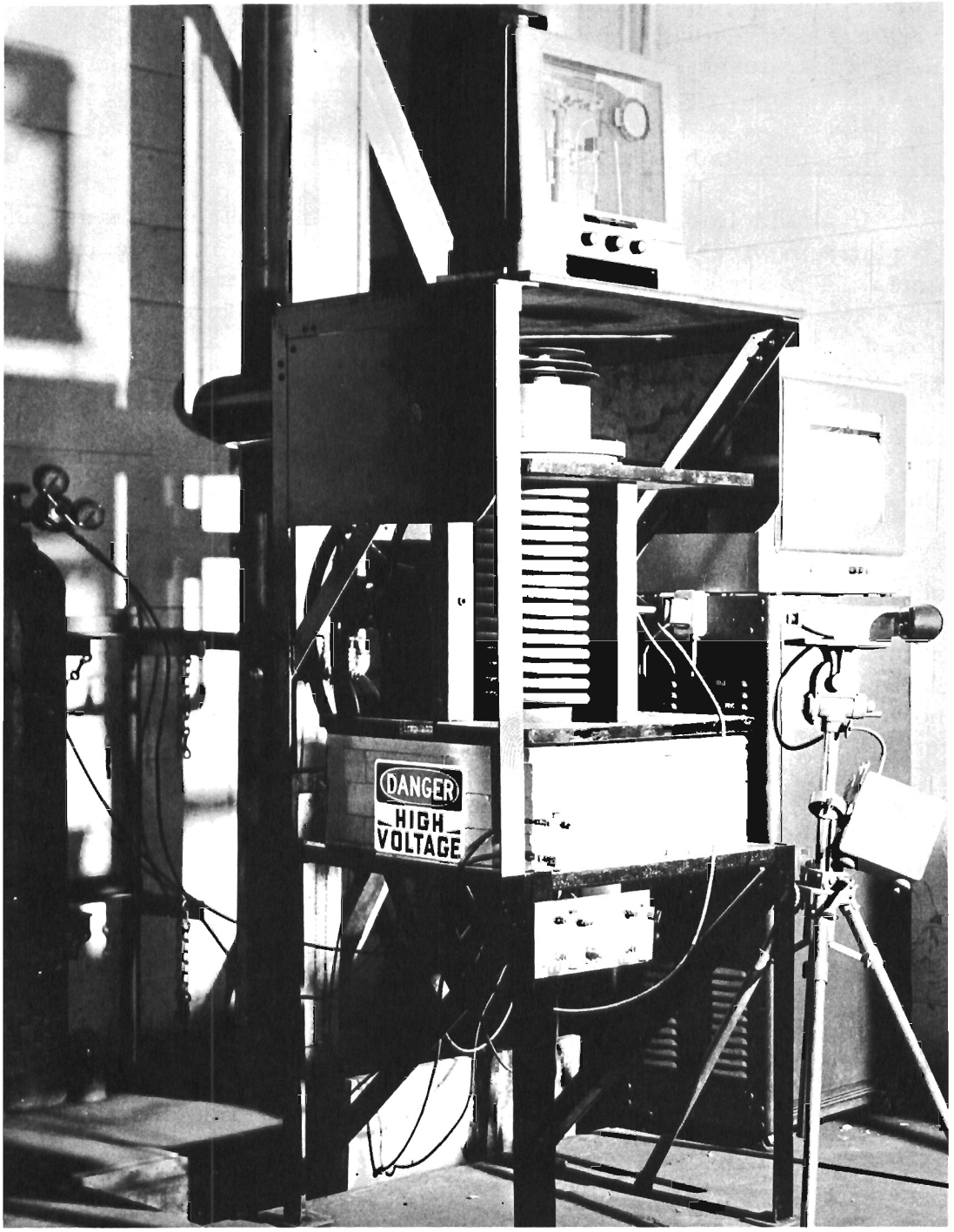

Figure 5. Oxidation Apparatus, Induction-Radiation Setup, Overall View

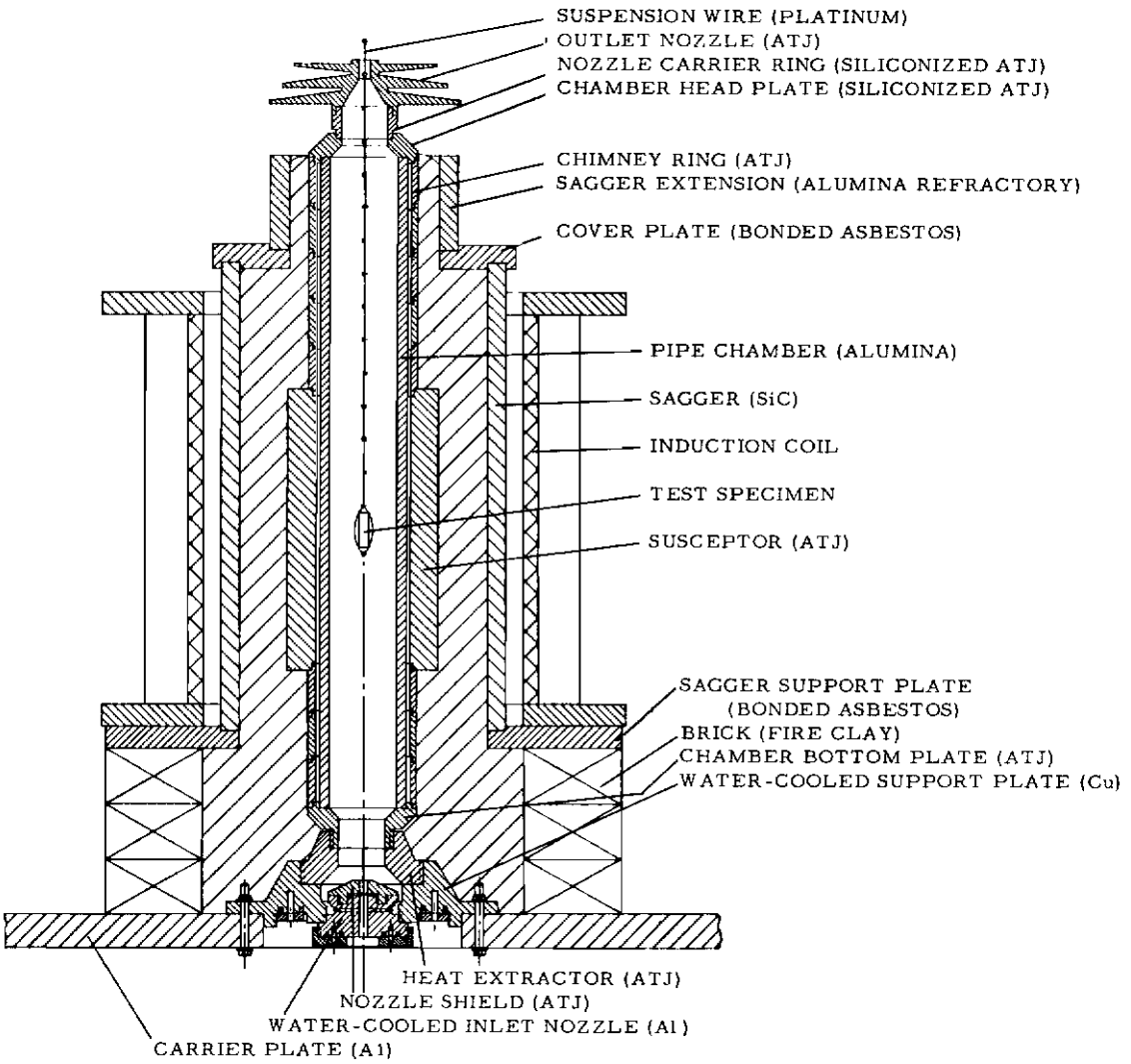

Figure 6. Oxidation Apparatus, Induction-Radiation Setup, Cross Section

4.1.2. Resistance Equipment

Resistance heating was considered as a method of providing oxidizing conditions at temperatures higher than those obtained with the induction-radiation setup described above. The resistance apparatus which was built is shown in Figure 7. A variable electric current which can be controlled precisely is passed directly through the test specimen held in water-cooled copper terminals. The surface temperature of the hot zone in the exposed portion of the specimen is measured by means of a 2-color pyrometer. Readings with such an instrument do not depend on the emissivity of the surface observed provided that grey body conditions prevail. Although the latter condition has not been checked in this study, it is believed that measurements with a 2-color pyrometer are more

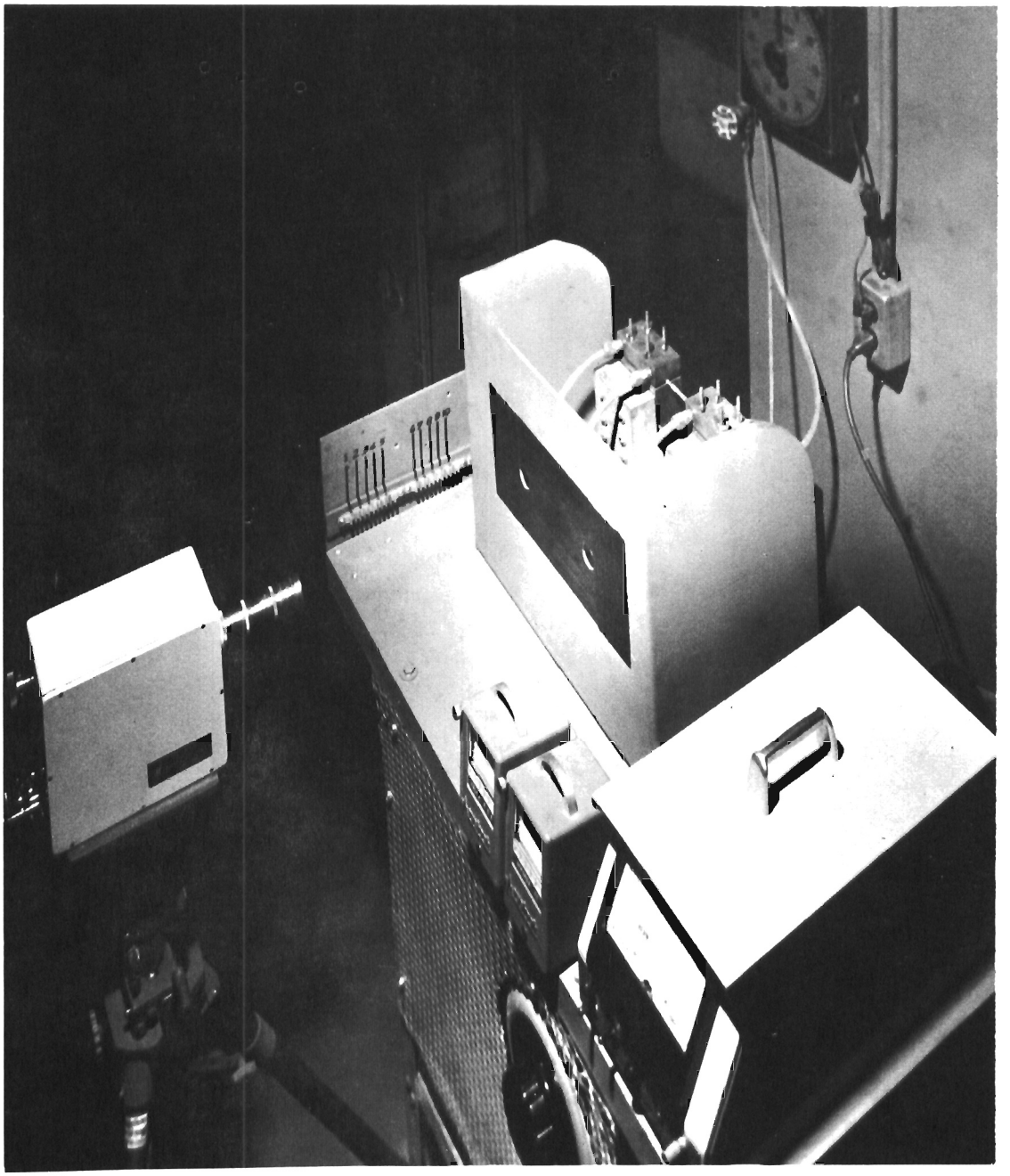

Figure 7. Oxidation Apparatus, Resistance Setup, Overall View

nearly true than values obtained with a standard optical pyrometer since the latter requires a black surface or its equivalent (non-black surface in an enclosure, both at the same temperature) neither one of which exists in the setup described.

The resistance-oxidation test has some inherent disadvantages. Large temperature gradients in the longitudinal direction result in a nonuniform surface temperature, thus ruling out weight change data of general usefulness, while gradients in the transverse direction produce severe conditions by maintaining the interior of the specimen at temperatures higher than those recorded on the surface. The test, nevertheless, is a good screening test for oxidation resistant coatings and composites because it is simple, is inexpensive, allows direct observation of the oxidation phenomena and is not limited in temperature.

4.1.3. Arc Image Equipment

Contrary to the conditions in the resistance setup explained in Section 4.1.2, most methods for measuring oxidation supply the heat to the outside of the specimen. An arc image furnace, shown in Figures 8 and 9, was used to produce this condition at high temperatures. In this setup, an ellipsoidal mirror system is used to transmit energy from an electric carbon arc to one plane surface of the sample being tested.

The equilibrium temperature reached by this surface depends primarily on the energy flux, on the condition of the surface, and on the thermal conductivity of the sample. The energy flux is adjusted by means of a shutter shown in the middle of the schematic diagram in Figure 9 and the temperature is measured by means of a calibrated photocell. The shutter controlling the radiation to the photocell is synchronized with the shutter in the middle between the mirrors but the phase difference is adjustable which permits two types of measurements to be made. In one-case, the shutter adjacent to the photocell opens when the shutter in the middle between the mirrors closes. Accordingly, only radiation emitted from the sample is measured. In the other case, both shutters are allowed to open simultaneously so that the photocell receives the radiation of the carbon arc as reflected by the sample in addition to the intrinsic sample radiation. A combination of both measurements can be used to derive spectral reflectance, spectral emittance, and the true temperature of the sample surface.

Weight change determinations obtained with this apparatus lack general usefulness since the nonirradiated surfaces of the sample exhibit considerably different temperatures. The arc image furnace, however, is of eminent value because it allows direct observation of oxidation

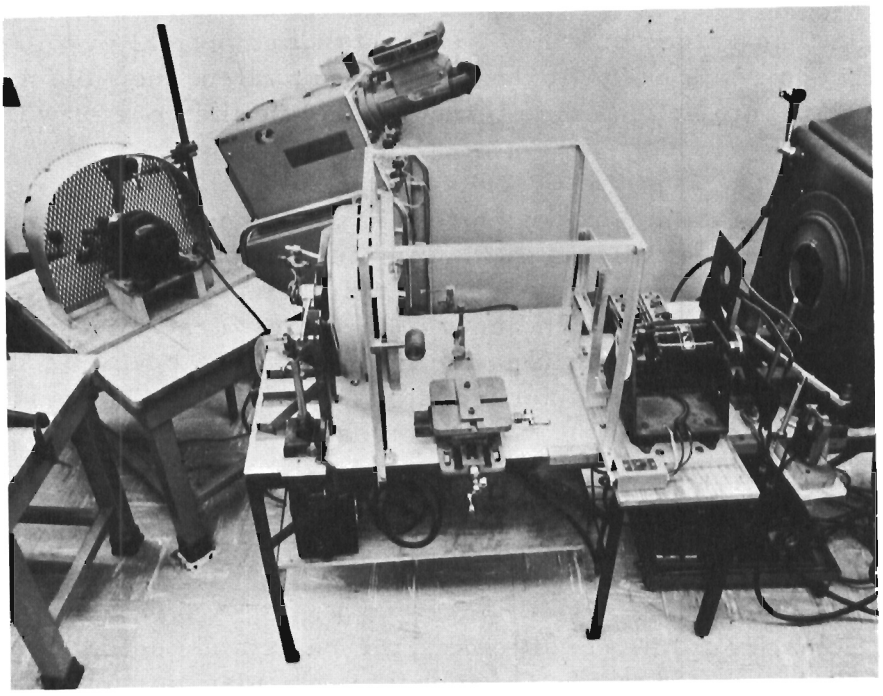

Figure 8. Oxidation Apparatus, Arc Image Setup, Overall View

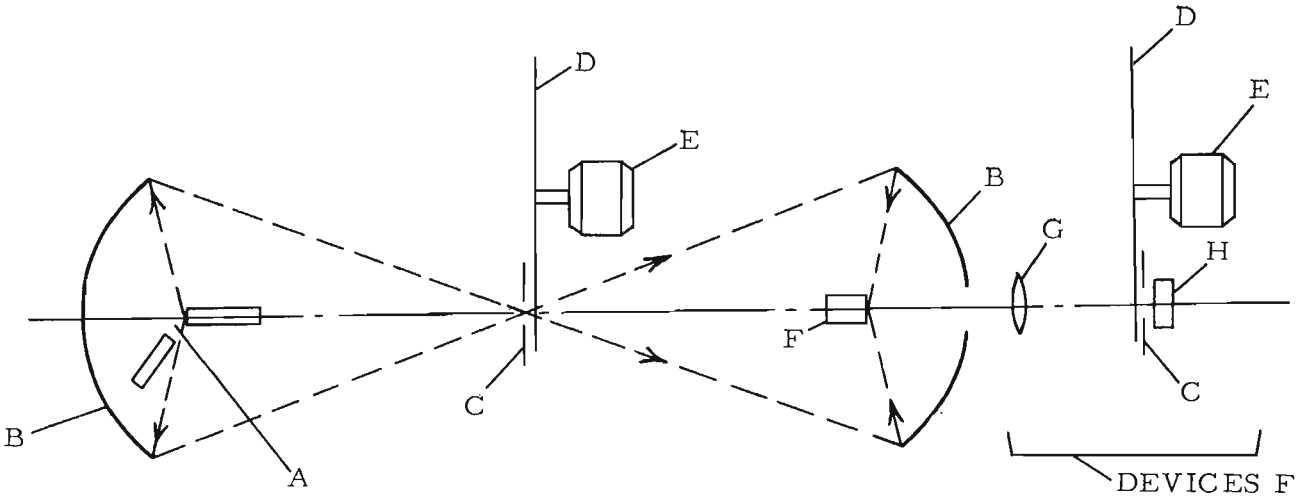

A - ELECTRIC ARC
B - ELLIPSOIDAL REFLECTOR
C - DIAPHRAGM
D - SHUTTER
E - MOTOR
F - SAMPLE
G - LENS
H - PHOTOCELL

Figure 9. Oxidation Apparatus, Arc Image Setup, Schematic Diagram

phenomena at high temperatures without introducing the errors caused by high internal temperatures obtained with resistance heating.

4.1.4. Levitation Equipment

The preceding sections have pointed out that both the resistance and the arc image methods for measuring oxidation are well capable of providing temperatures high enough for any practical demand but that weight change data derived from these tests can have no more than relative significance. On the other hand, the induction-radiation method is capable of yielding useful weight change data but its range does not include high enough temperatures. Consequently, there was need for an apparatus which could combine technically useful weight change data with high temperatures. The answer to this need is a method involving rotational levitation of the test specimen by means of an electromagnetic field which can be used because all graphite base composites of interest in this study exhibit a reasonably good electrical conductivity.

Figure 10 shows the resulting setup in operation. At the time of this writing, development of the apparatus is not complete because devices for fully automatic temperature control are being constructed. Consequently, there is no oxidation data obtained with this apparatus to be presented in this report. Discussion of the setup has been included here for the sake of completeness regarding the survey of oxidation test developments conducted.

A complete discussion of the levitation theory and design is given in Appendix I.

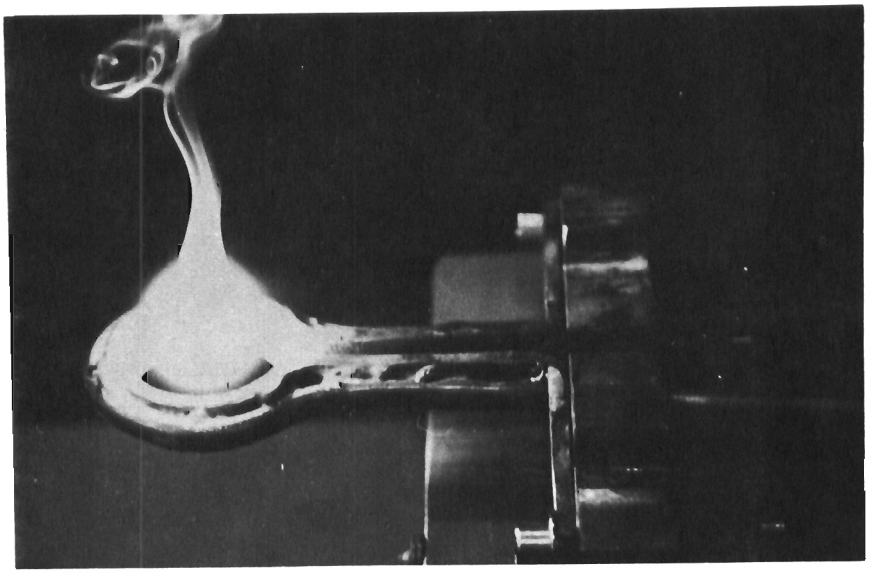

Figure 10. Oxidation Apparatus, Levitation Setup, in Operation

4.2. Strength Measurements

Equipment for performing tensile strength measurements at elevated temperatures is available; however, in the case of brittle materials, tensile strength measurements are extremely sensitive to misalignment of the specimen within the holders which causes considerable scattering of results and a large number of tests are required to produce meaningful data. It was decided, therefore, to measure flexural strength which is a much more simple measurement to make. An apparatus shown in Figures 11 and 12 was constructed to measure flexural strength at elevated temperatures. The breaking force is supplied by an air cylinder. The testing fixture is enclosed by lampblack powder and heating is accomplished by induction. This basic setup is quite similar to the fabricating equipment described earlier. Critical load elements are made of ZTA graphite because of its high compressive strength and low compressive creep in the across-grain direction. The apparatus was proven to be operational for temperatures up to 3400°C.

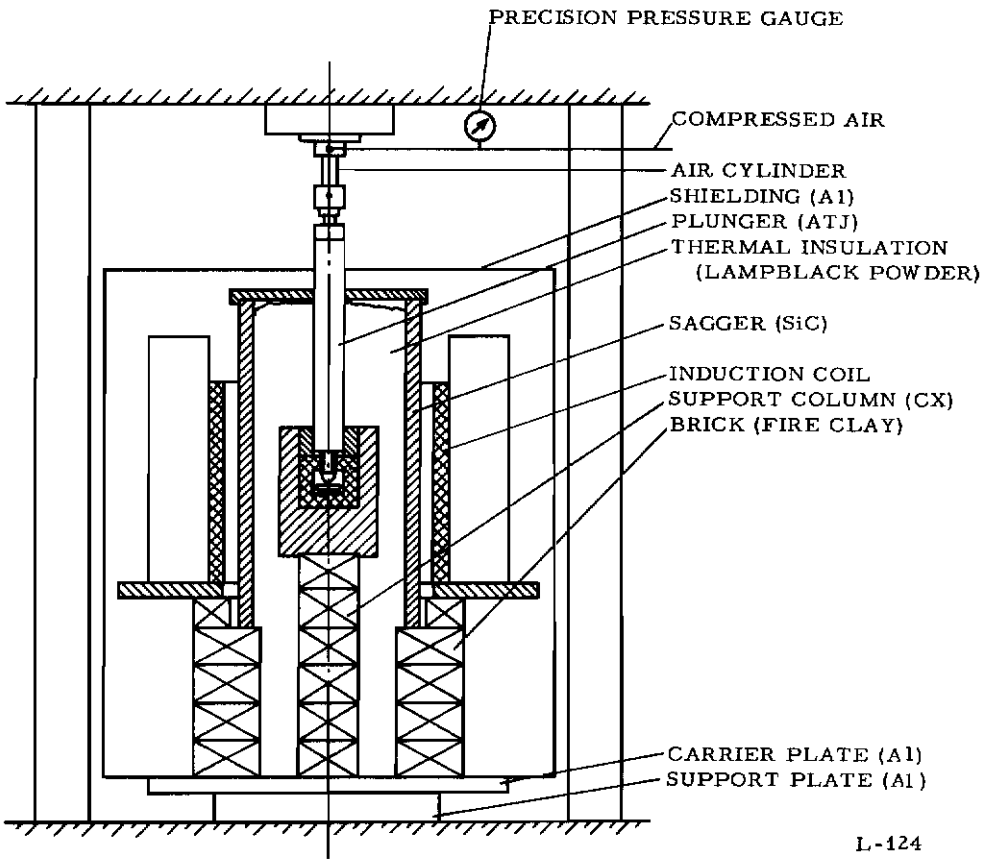

Figure 11. Apparatus for the Determination of Flexural Strength at High Temperatures, Total Cross Section

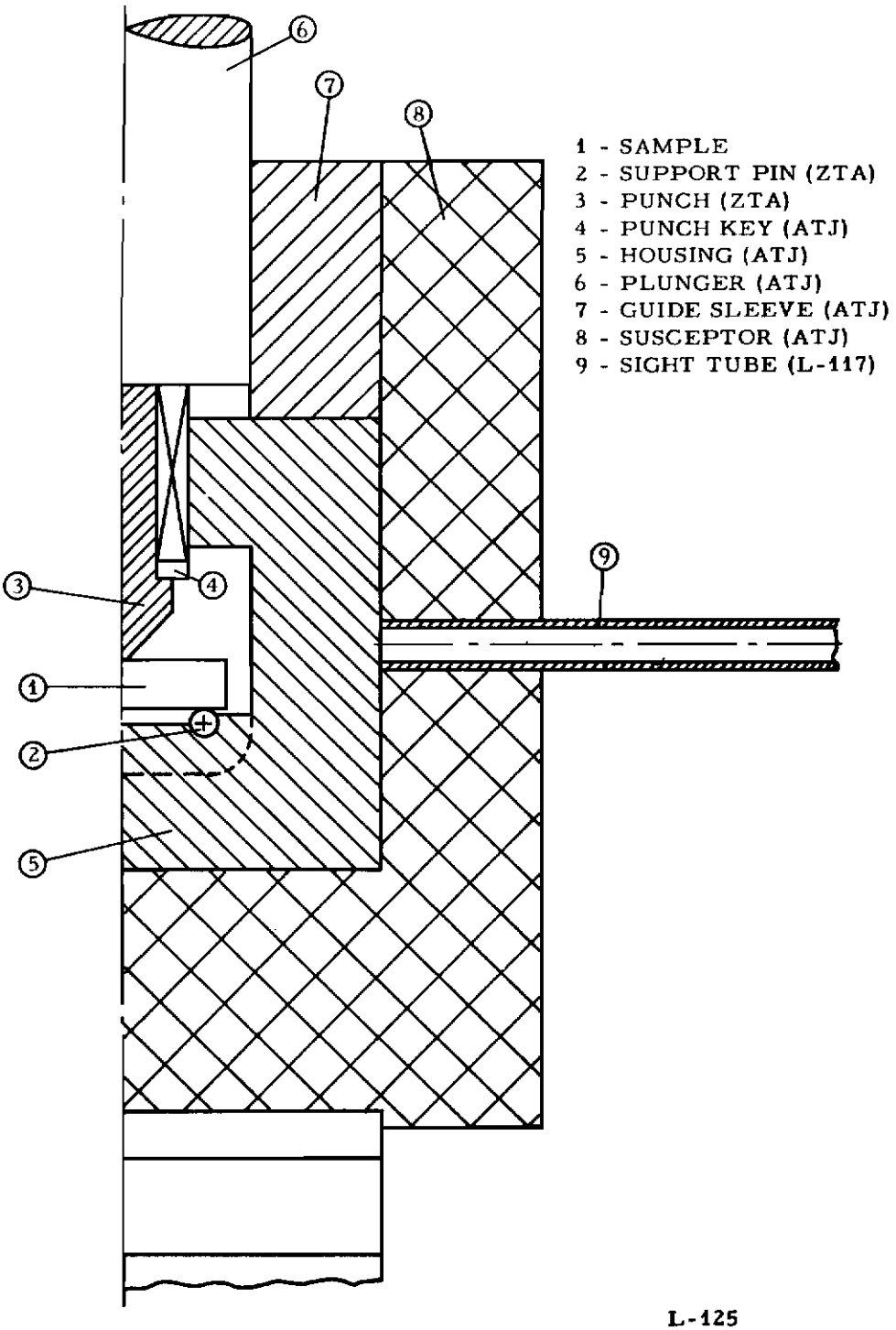

Figure 12. Apparatus for the Determination of Flexural Strength at High Temperatures, Detailed Cross Section of Breaking Fixture

4.3. Thermal Expansion Measurements

Coefficients of thermal expansion were measured by heating test specimens in a graphite tube furnace while observing their dimensional changes through calibrated telescopes. A detailed description of the method is presented in WADD Technical Report 61-72, Volume XXVI, "Physical Properties of Some Newly Developed Graphite Grades", by R. B. Dull.

4.4. Thermal Conductivity Measurements

High temperature thermal conductivities were determined by the rectangular bar method. Details of this technique have been described by Doar and Pike in the Proceedings of the Fifth Conference on Carbon, Volume 2, p. 311, 1961.

4.5. Electrical Resistivity Measurements

High temperature electrical resistivities were obtained by passing a current through a cylindrical specimen and determining the voltage across the uniformly heated center section. A comprehensive description of the apparatus is given in ERC Report No. 262, National Carbon Company Research Laboratories, Parma, Ohio, by H. A. Downey and E. Micinski.

5. SEQUENCE OF DEVELOPMENTS AND RESULTING PRODUCT PROPERTIES

The work on graphite-refractory composites was started with investigations of binary and pseudobinary systems. Additives studied were boron carbide, hafnium, tantalum, columbium, zirconium carbide, titanium diboride, and silicon. In general, the process was carried beyond the melting point of the additive to further alloying.

The most promising oxidation protection was found to be provided by additives containing boron. Figure 13 illustrates the effect of TiB_2 additions to graphite as reflected in the oxidation rate at 800°C. Significant improvements were achieved with relatively small additive levels but no further gains resulted at higher levels. The oxidation rate, in all cases, was found to exhibit little or no dependence on time. This meant that while the oxidation rates were reduced, the oxidation process as such could not be halted.

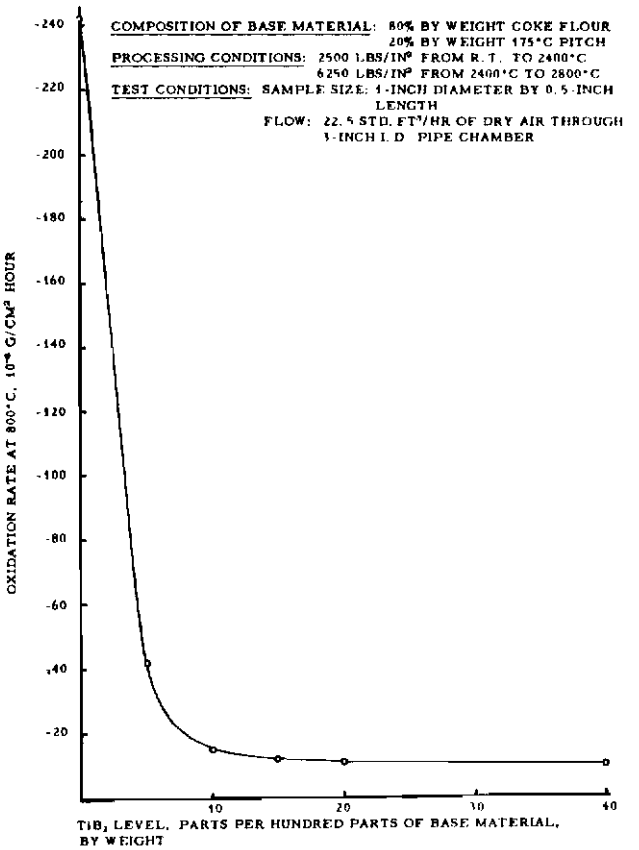

Figure 13. Effect of TiB_2 Additions to Graphite, Oxidation Rate at 800°C versus Additive Level

Effects of the additives on the strength of the material was more significant and satisfactory than on the oxidation rate. The flexural strength of two typical composites of this series as a function of temperature is given in Figures 14 and 15 and shows that a strong dependence on the grain orientation exists. This anisotropy is not detrimental since the maximum strength of such an anisotropic material is higher than the overall strength of an isotropic form of similar material and it is usually a simple matter to design a structural part in such a way as to utilize the maximum strength of the material.

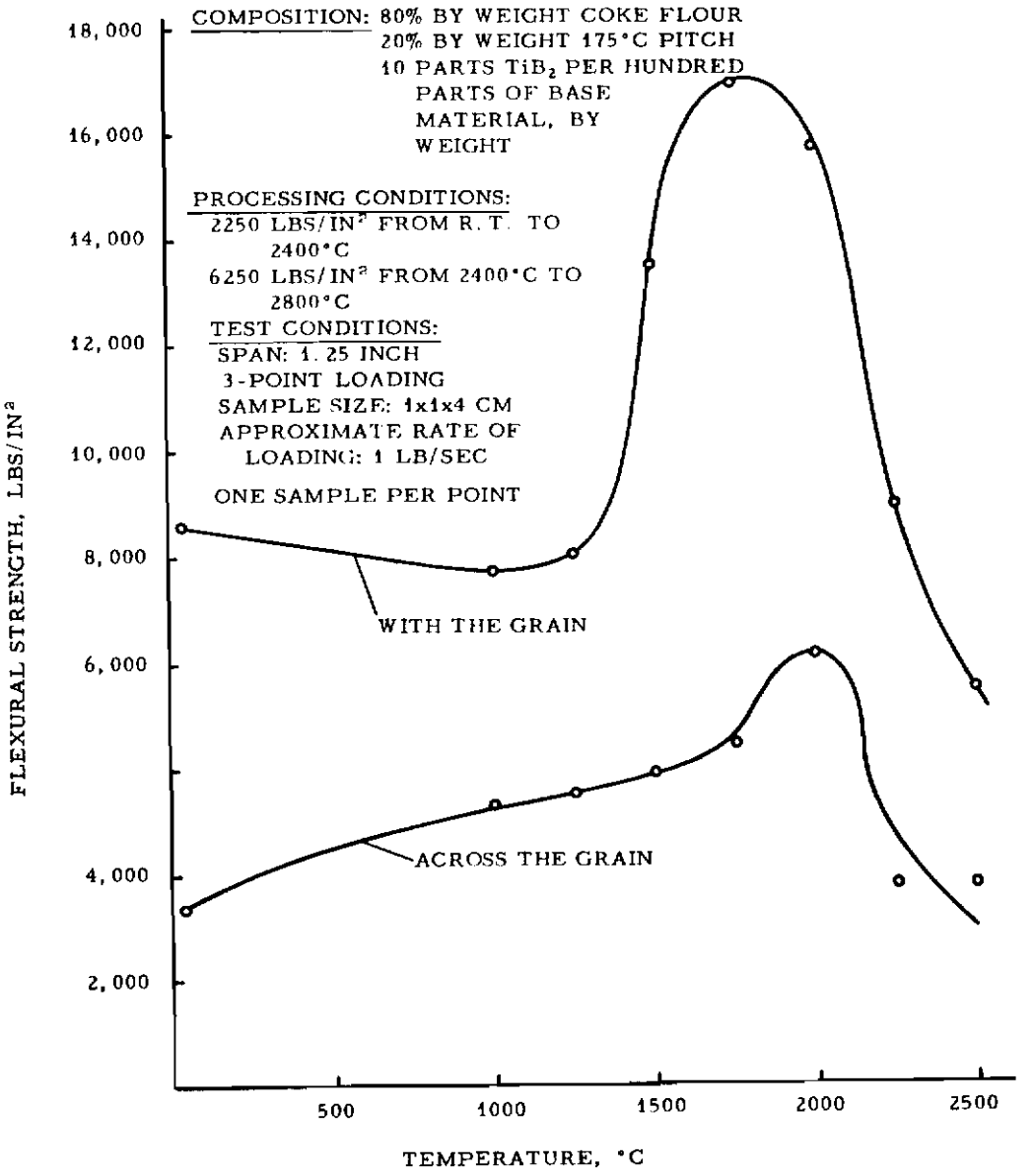

Figure 14. Flexural Strength of a C/TiB_2 Composite versus Temperature

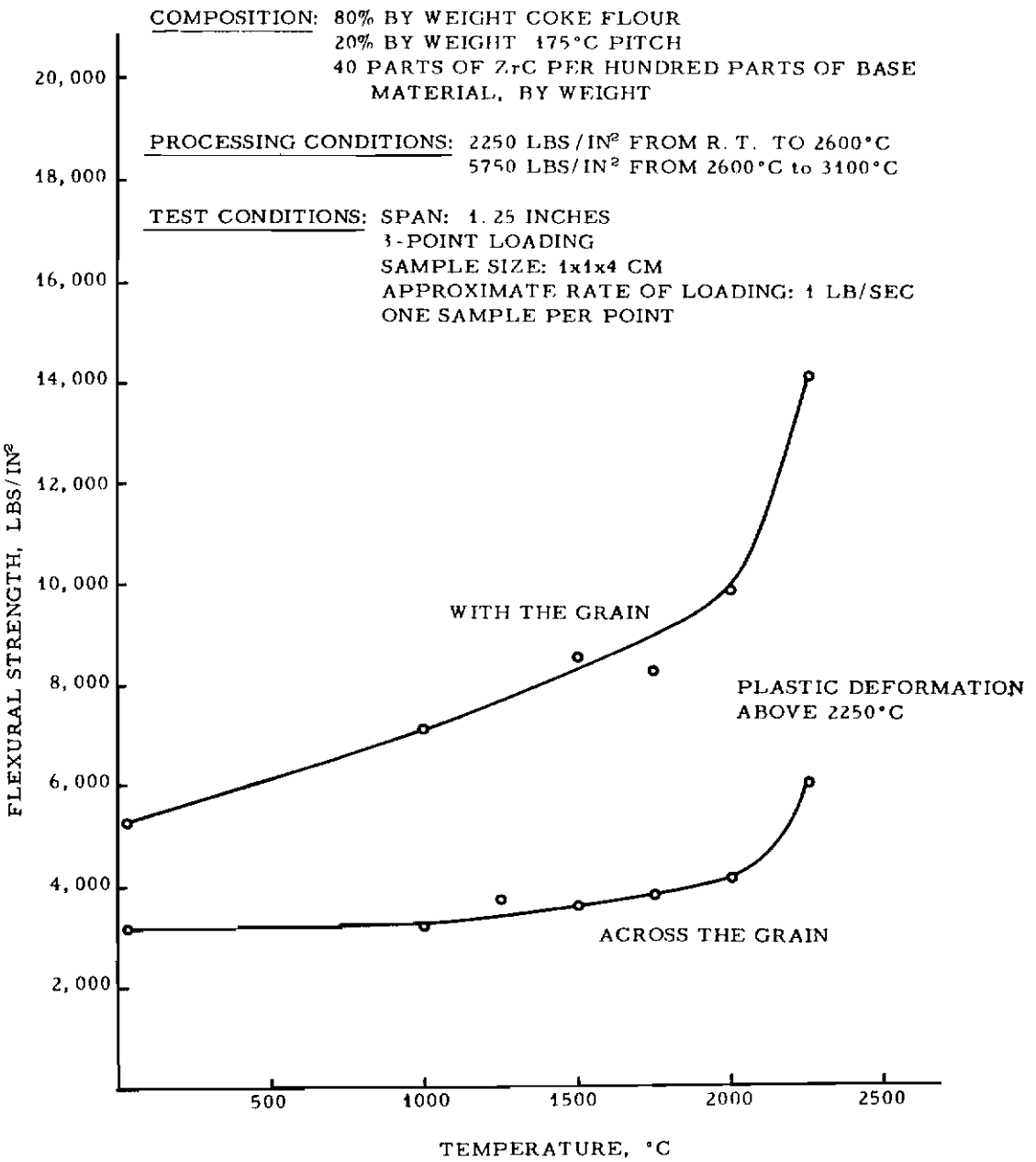

Figure 15. Flexural Strength of a C/ZrC Composite versus Temperature

Comparing the C/TiB_2 refractory composite (Figure 14) with a standard graphite such as ATJ indicates that an additive level of no more than 10 parts per hundred parts by weight of carbonaceous base material provided strength improvements of several hundred per cent up to a temperature of 2000°C. In the C/ZrC system, (Figure 15), an additive level of 40 parts per hundred parts by weight of carbonaceous base material was less effective than one quarter of this concentration in case of the C/Ti/B_2 system. This was attributed to the fact that at 2800°C liquid

TiB_2 dissolves graphite most readily whereas the ZrC does not dissolve graphite. Evidence of this is given in Figure 16 where, at the testing temperature, droplets of liquid TiB_2 were shown to "eat" holes into ATJ graphite but no such behavior was observed for ZrC droplets. The technical ZrC grade employed melted around 2900°C. At 3100°C, droplets of this material remained on the graphite surface, and were removed after solidification without much force or evidence of graphite dissolution.

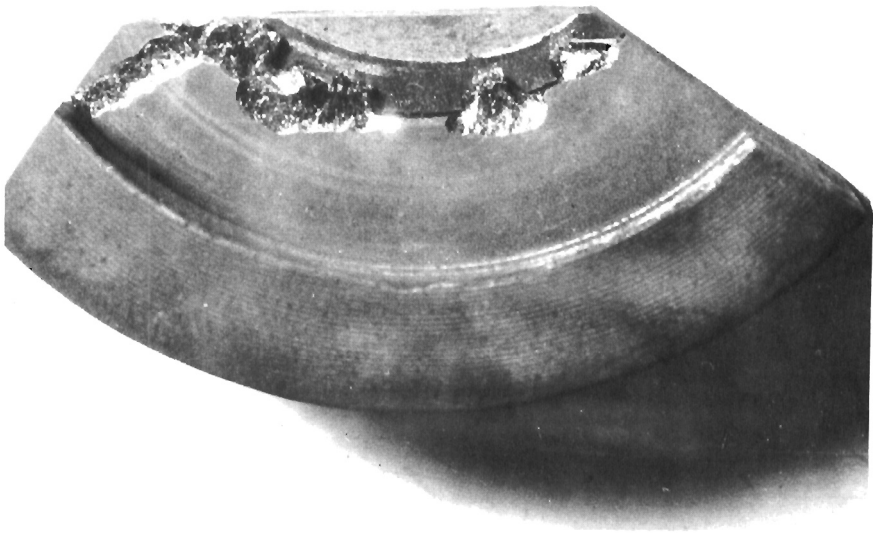

Figure 16. Effect of Molten TiB_2 on ATJ Graphite

The threshold of strength increase in the C/ZrC system, on the other hand, lies at a higher temperature than for the C/TiB_2 system (see Figure 15) and, if there is a maximum, it could not be determined in these experiments because of the plasticity of the composite material above 2500°C. The plasticity of this material is depicted in Figure 17 which shows a C/ZrC composite sample after an attempt to break it at 2500°C (upper picture) as compared with a sample of ATJ graphite broken at 2750°C (lower picture). The rate of loading was the same in both cases. It can be noted that the graphite specimen fractured after some plastic deformation in spite of the higher temperature while the composite sample was forged to the geometric limits of the test appa-

ratus without any signs of fracture. Plasticity of this type may be of advantage for structural applications where brittleness of graphite is a problem.

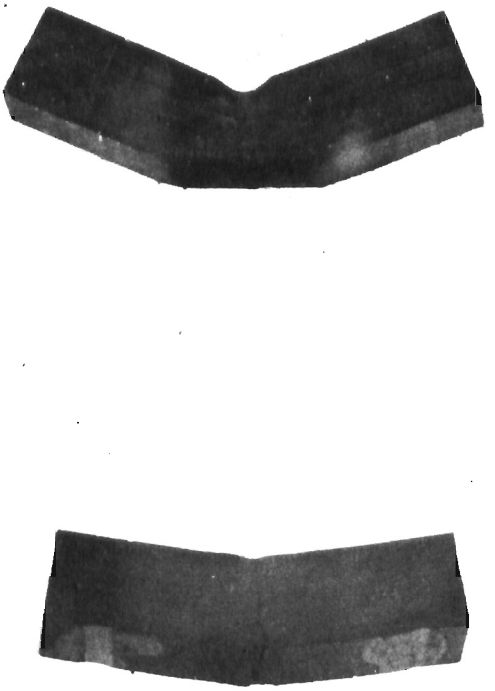

Figure 17. High Temperature Plasticity Comparison, C/ZrC Composite versus ATJ Graphite

In view of the unsatisfactory oxidation results with binary and pseudobinary systems, subsequent work shifted to ternary systems. First trials with an additive combination of B_4C and Si indicated that such systems produced composites capable of resisting oxidation by forming a protective coating from their own oxidation products. This is illustrated in Figure 18 which shows the oxidation characteristic of such a C/B_4C/Si composite for a temperature of 1200°C as compared with a pseudobinary system of the earlier series and with ATJ graphite. It is seen that, after an initial fast weight loss, the C/B_4C/Si composite tended to become stable and to not be affected further by oxidation.

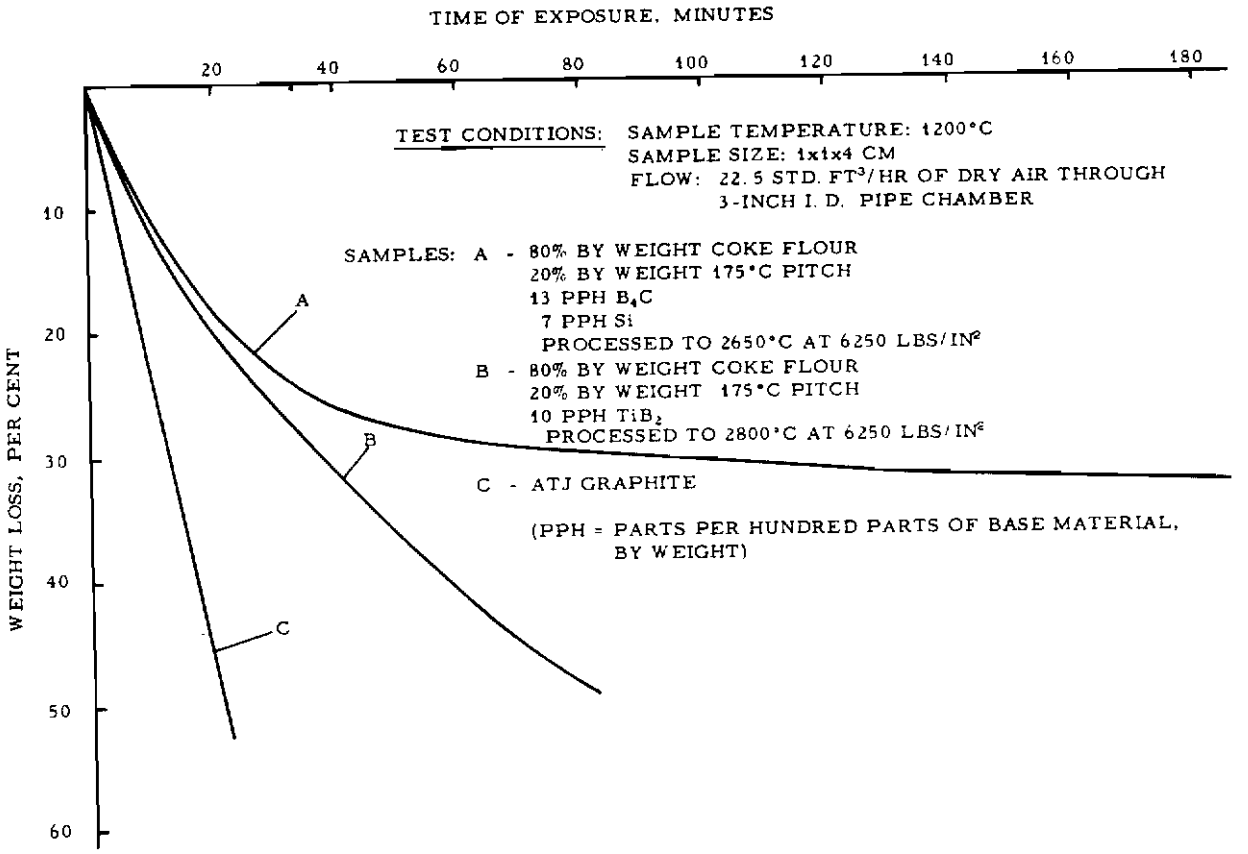

Figure 18. Oxidation Characteristics at 1200°C, C/B_4C/Si, C/TiB_2, ATJ

Studies were extended to materials containing three and more elements besides carbon. On the basis of the promising performance of the C/B_4C/Si system, the boron and silicon were retained while other elements having oxides of high melting point were also included. There was a good reason for choosing elements of the latter type as a part of the additive combination. At 1200°C and above, the coatings formed by the C/B_4C/Si system were found to be quite liquid as evidenced by the fact that droplets would form at the bottom of the sample. In other

words, the coating was liquid enough to flow downwards under the influence of gravity and to thus expose the upper regions of the sample before sufficient coverage by a newly formed coating could become effective. The addition of elements with oxides of high melting point was expected to increase the viscosity of the coating to the point where this difficulty would be overcome. This theory was confirmed by various $C/TiB_2/Si$ systems for temperatures up to approximately 1550°C. Figure 19 illustrates the oxidation behavior of one such material at 1200°C as compared with the previously characterized $C/B_4C/Si$ composite and shows that steady state conditions essentially were achieved by the $C/TiB_2/Si$ system. The next trials were made to determine whether silicon was actually necessary in such a system. Figures 20 and 21 depict the results of oxidation tests on C/TiB_2 systems with varying amounts of silicon, at temperatures of 1200 and 1550°C, and clearly indicate the necessity of the Si in the system.

When the $C/TiB_2/Si$ system was tested at temperatures above 1550°C, droplets of molten material began to form on and drop off the surface of the sample which resulted in a sharp decrease in the oxidation resistance of the composite.

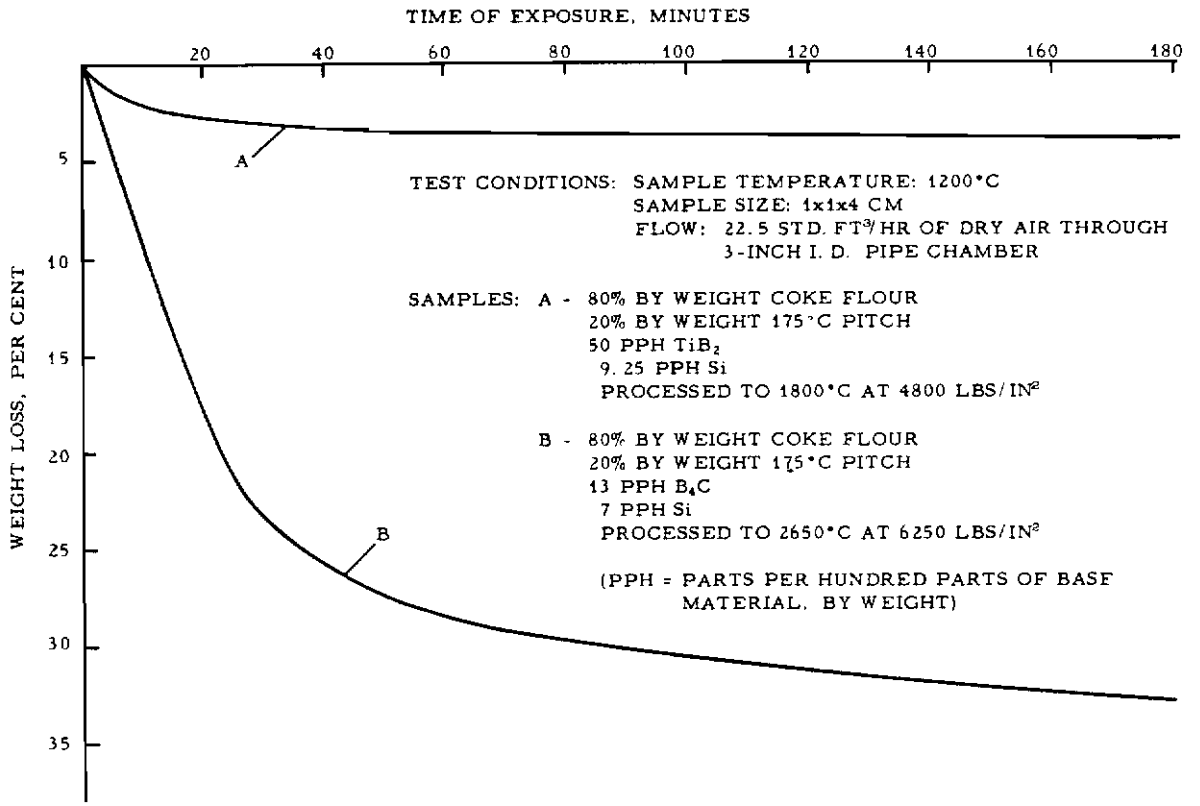

Figure 19. Oxidation Characteristics at 1200°C, $C/TiB_2/Si$ versus $C/B_4C/Si$

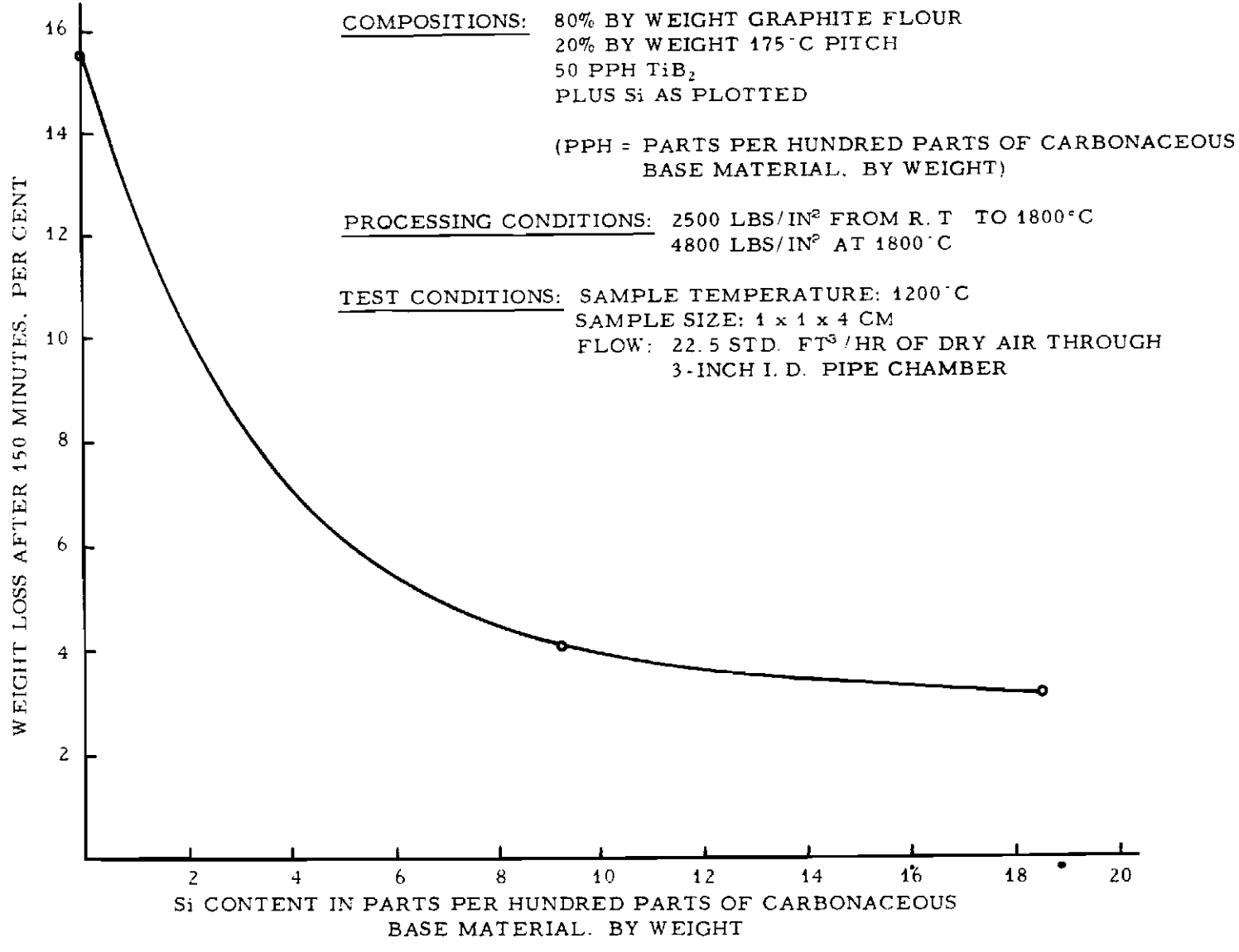

Figure 20. Effect of Silicon on C/TiB_2 Composites, Oxidation Rate at 1200°C versus Silicon Level

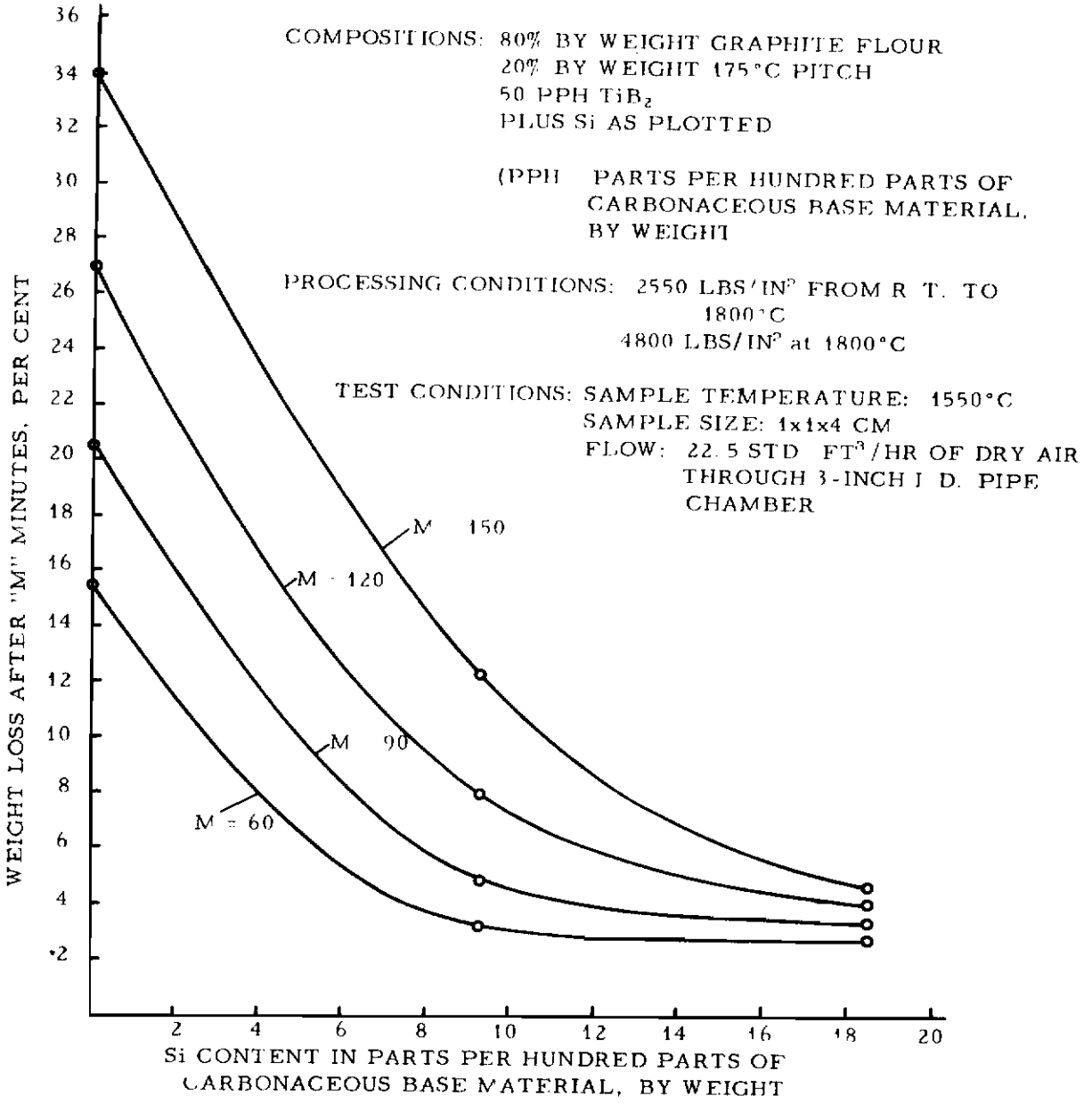

Figure 21. Effect of Silicon on C/TiB_2 Composites, Oxidation Rate at 1550°C versus Silicon Level

It was decided, therefore, to replace TiB_2 by ZrB_2 since zirconium oxide has one of the highest melting points of all oxides. This system provided protection against oxidation to temperatures in excess of 2000°C. A $C/ZrB_2/Si$ composite, formerly referred to as experimental grade JT-0832 and presently referred to as grade JTA, has been submitted to rather extensive testing. Its isothermal oxidation behavior at various temperatures and under various test conditions is illustrated in Figures 22, 23, and 24, while Figures 25, 26, 27, and 28 depict flexural strength, thermal conductivity, electrical resistivity, and coefficient of thermal expansion as a function of temperature. In all of these graphs, pertinent corresponding characteristics of graphite are included for comparison.

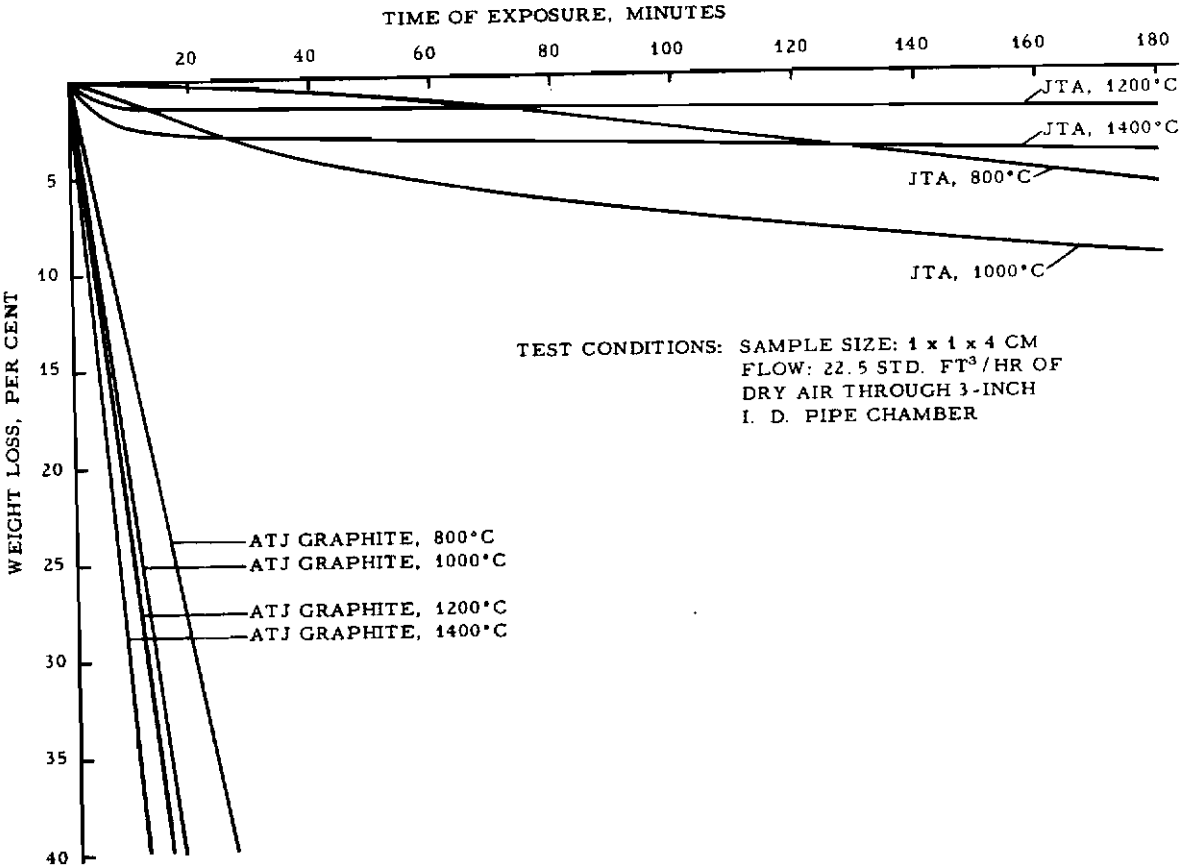

Figure 22. Oxidation Characteristics of JTA as Determined in the Induction-Radiation Setup

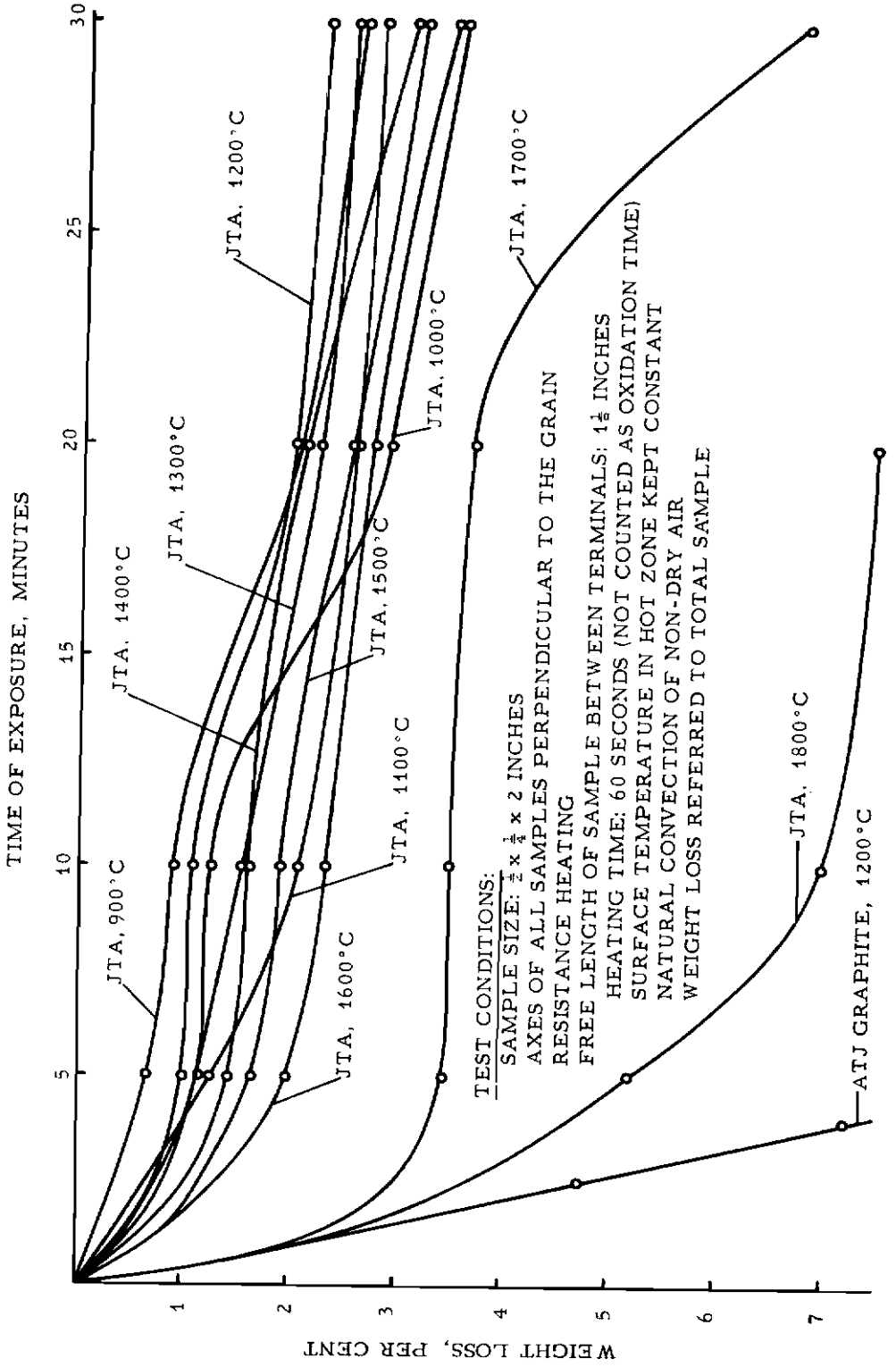

Figure 23. Oxidation Characteristics of JTA as Determined in the Resistance Setup

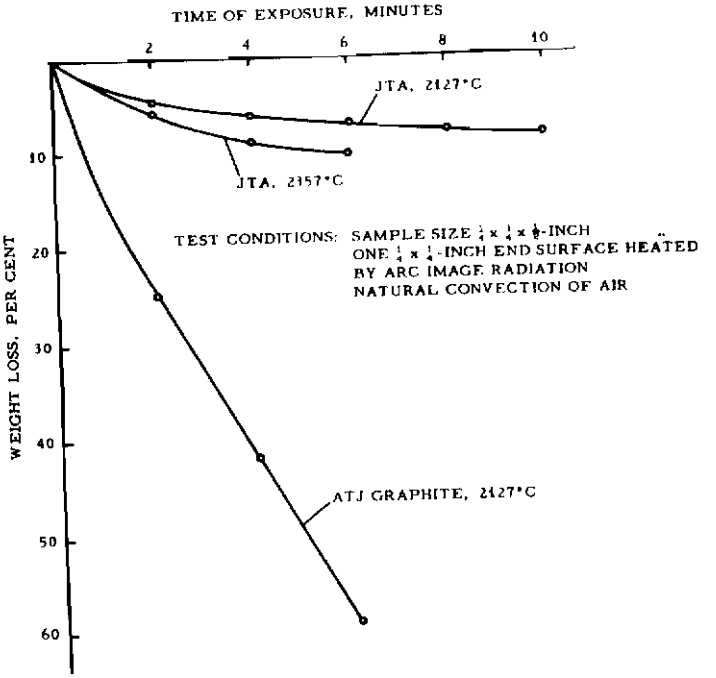

Figure 24. Oxidation Characteristics of JTA as Determined in the Arc Image Setup

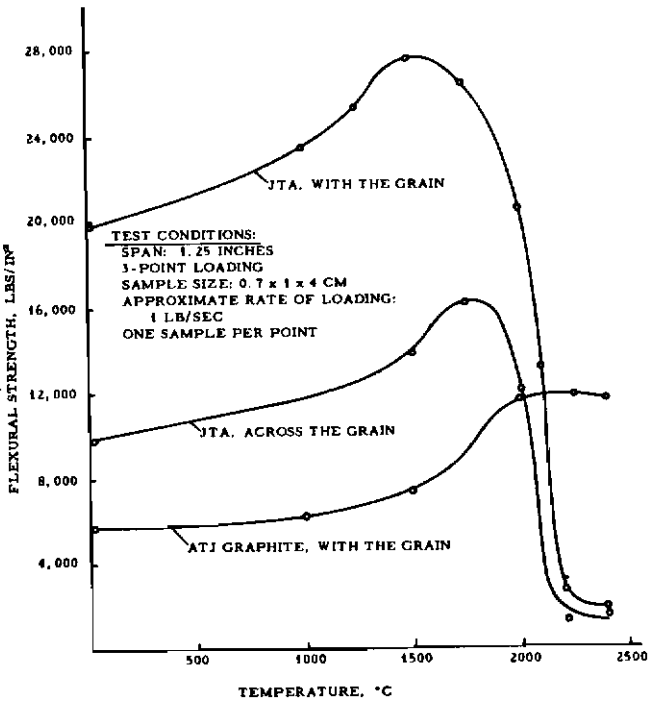

Figure 25. Flexural Strength of JTA versus Temperature

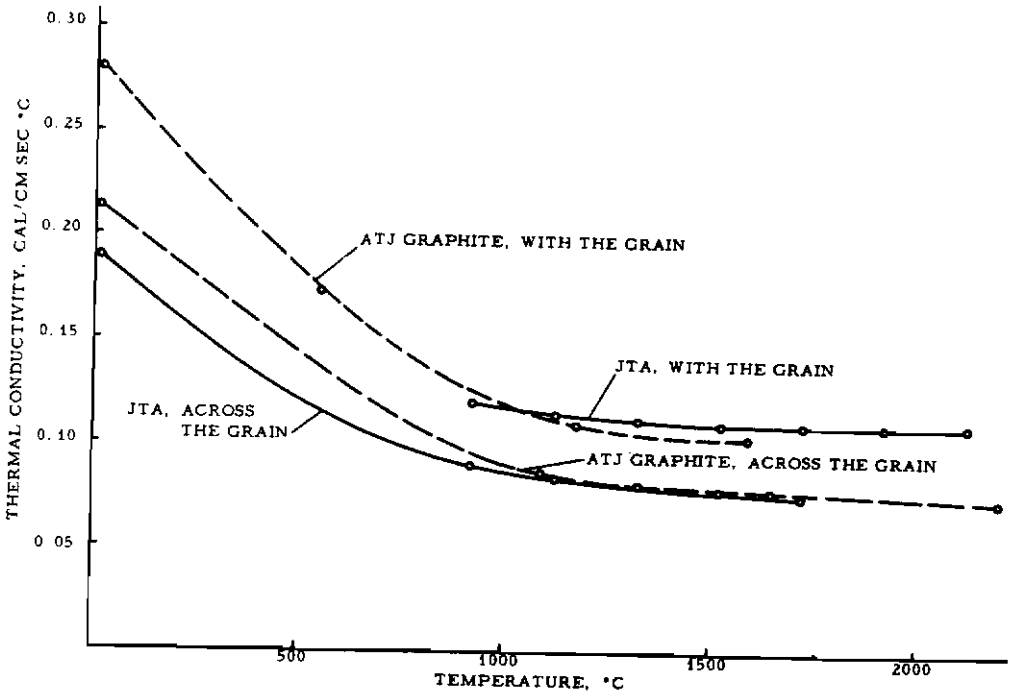

Figure 26. Thermal Conductivity of JTA versus Temperature

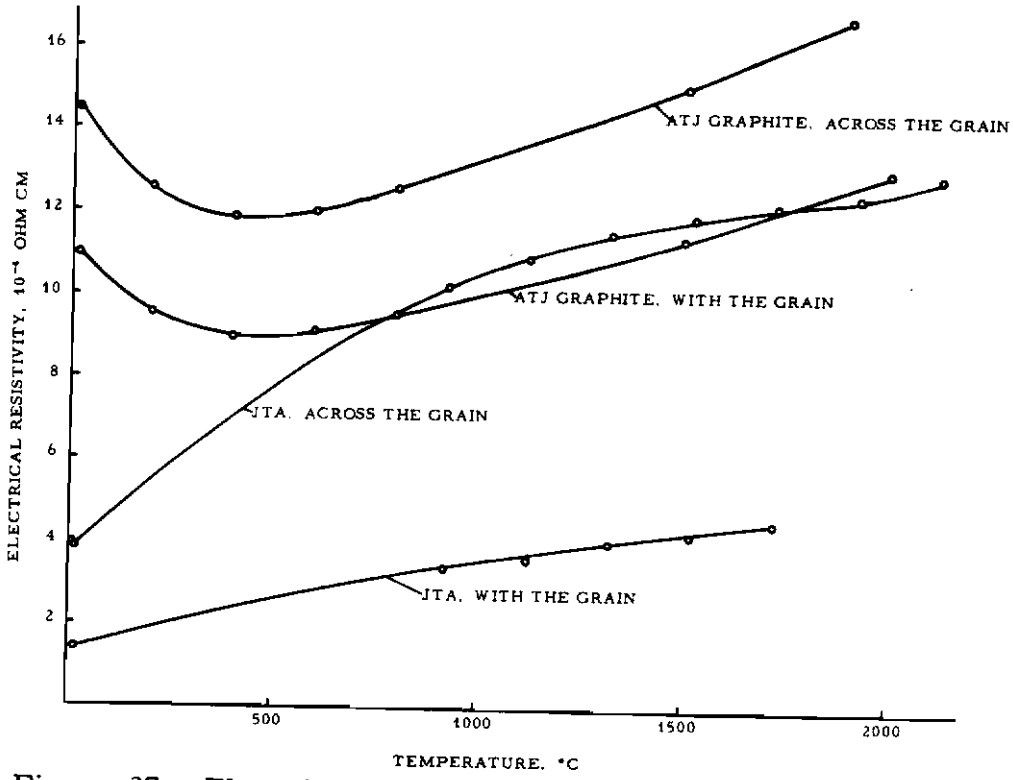

Figure 27. Electrical Resistivity of JTA versus Temperature

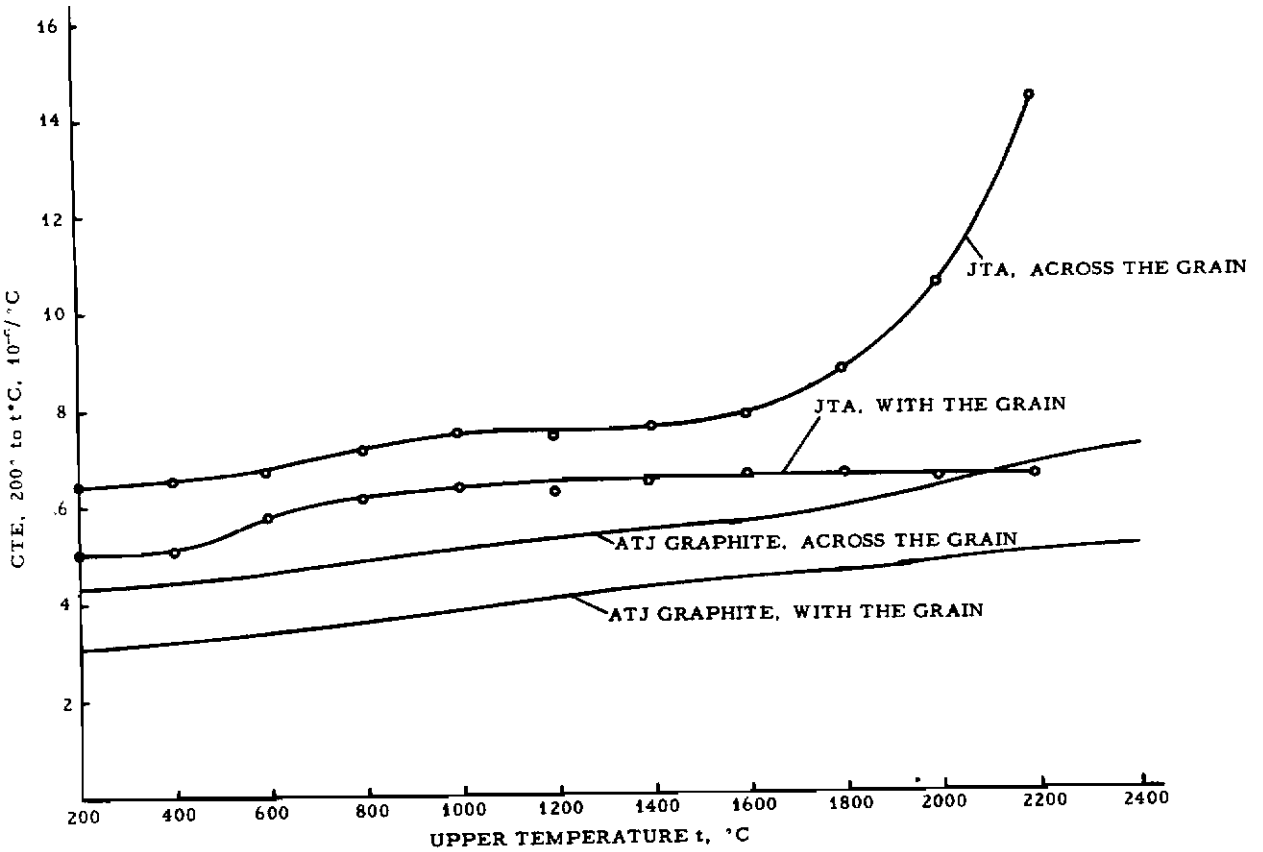

Figure 28. Coefficient of Thermal Expansion of JTA versus Temperature

X-ray analyses showed JTA to consist of graphite, ZrB_2, and alpha-SiC. No ternary or quaternary compound was identified. Above 2200°C, a liquid phase appeared in the system. While the composition of this liquid phase was not investigated, related experiments have shown that the ZrB_2/SiC is a pseudobinary system, and that its alloys are capable of dissolving very sizable amounts of carbon. It is reasonable to assume that the liquid phase in question consists of zirconium diboride, silicon carbide, and carbon.

The oxidation resistance of JTA is provided by the formation of coherent coatings of highly refractory solid solutions of oxides on the exposed surface. In Figure 29, the cross section of such a coating formed at 2000°C is viewed in partially polarized light at a magnification of 100X. The surface of the specimen is covered by two distinct layers; the outer layer undoubtedly consists of oxides while the inner one is believed to be partially oxidized composite material serving as a diffusion barrier between the oxides and the base from which they were formed. Droplets of liquid phases do not appear on the surface of this composite under ordinary oxidation test conditions except at very high temperatures.

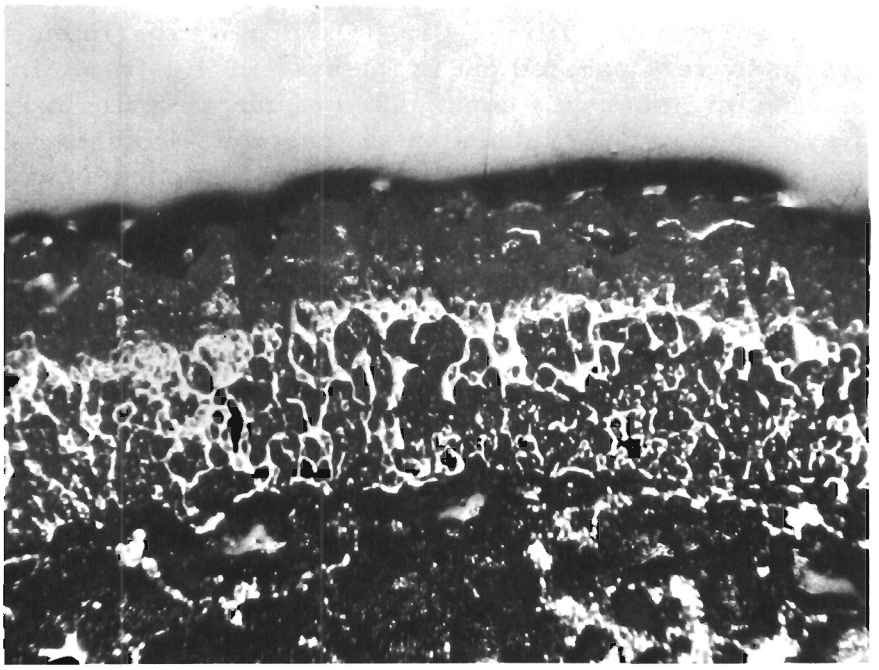

Figure 29. Structure of JTA Coating, Formed at 2000°C Viewed in Partially Polarized Light, 100X Magnification

During the high temperature testing or use of the JTA composite, the oxidation of ZrB_2 can be expected to yield sizable amounts of B_2O_3 which, by itself, melts at 450°C. In spite of this, the C/ZrB_2/Si system performs well at high temperatures because part of the B_2O_3 from the oxidation of ZrB_2 combines with the other materials present to form solid solutions with high melting points and the rest of the B_2O_3 evaporates. The same applies to SiO_2 formed in the JTA coating by the oxidation of the contained SiC. Zirconium oxide, a coproduct of B_2O_3 in the oxidation of ZrB_2, which does not evaporate to any significant extent, represents the primary coating constituent and is bonded together by solid solutions of ZrO_2, SiO_2 and/or B_2O_3. A specimen of JTA, preoxidized at 1200°C and subsequently heated in a mass spectrometer to a temperature of 1250°C under a pressure of 5×10^{-5} torr, revealed SiO, B_2O_2, and B_2O_3 to be the primary vapor species. These gases appeared in about equal quantities. A careful check was made for ZrO (gas) and ZrO_2 (gas) but neither was found to be present.

In view of the above findings, the oxidation behavior of JTA at reduced air pressure was considered of interest. Under such conditions, less oxygen is available on the surface of the material but all rates of evaporation increase with decreasing pressure because, in accordance with the Langmuir theories, less vaporized molecules are

returned by the surrounding film of gas. Oxidation experiments at reduced pressures were carried out in the system illustrated in Figure 30. The reaction chamber was constructed of quartz tubing having an inside diameter of about 2 inches and a length of 11 inches. The air input was metered at atmospheric pressure. A sectioned support rod consisting of glass, boron nitride, and graphite was used to suspend the test specimen in the reaction chamber. The whole setup was then installed in the previously described arc image furnace in such a way that the arc image impinged on the sample face pointing to the air inlet. The temperature of this surface was used as the thermal parameter since it represented the hottest zone of the specimen.

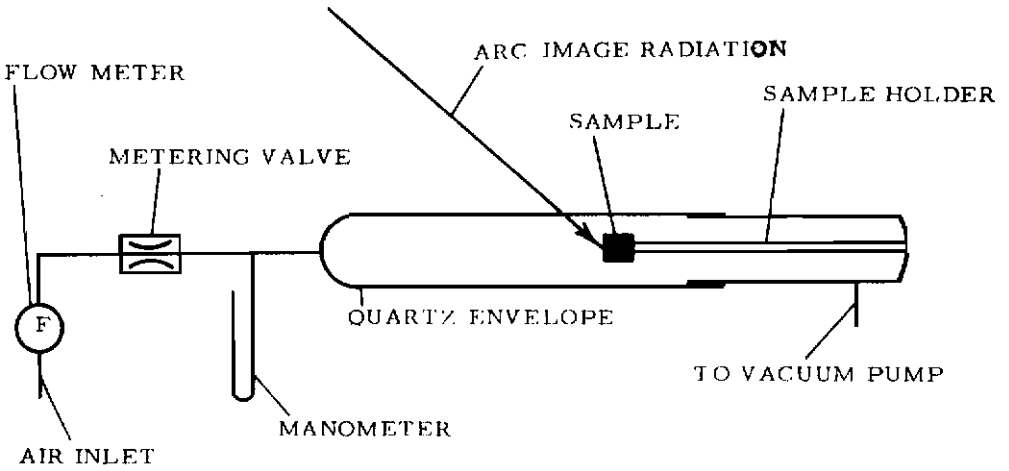

Figure 30. Apparatus for Oxidation Studies at Reduced Pressures

Results of these low-pressure oxidation experiments are illustrated in Figure 31 where the weight loss of the sample is plotted as a function of the exposure time with the chamber pressure serving as parameter. The rate of oxidation, at the test temperature of 2350 ± 150°C, decreased with decreasing pressure which indicates that evaporation is a less significant factor than availability of oxygen.

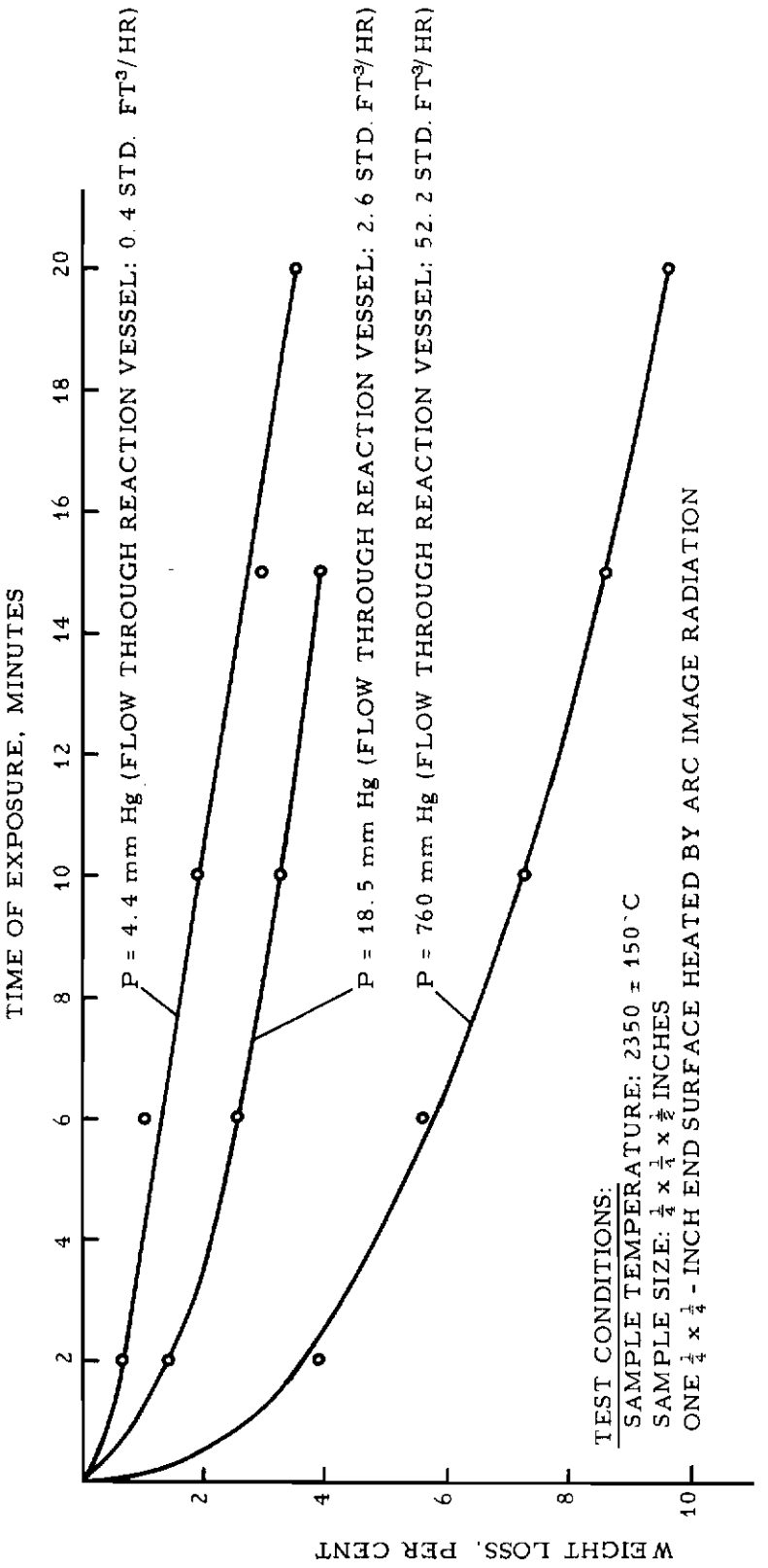

Figure 31. Oxidation Characteristics of JTA at 2350°C for Various Air Pressures

Grade JTA was found to be less oxidation resistant at 1000° than at 1200°C (Figure 23) indicating that the effectiveness of the protective coating as a function of temperature could not be predicted. It was conceivable that a material which performed well at two temperatures A and B, might oxidize catastrophically at a temperature C between A and B. In other words, if each oxidation test were performed under isothermal conditions, a great many temperature levels would have to be investigated to avoid misconclusions. This not only would require many samples - which is a point of serious concern where costly materials are studied - but also would be a lengthy procedure because of the time required to achieve thermal equilibrium in the furnace (induction radiation setup) for the various temperature levels. Since the composition and preparation of each new composite material was to be based on the results of the preceding one, it would be necessary to test each composite at all temperature levels of interest before proceeding to the next formulation. As a result of the above conditions progress would be impeded and guesswork encouraged by the temptation of cutting the number of temperature levels to a minimum.

A dynamic type of oxidation test which allowed relatively fast and yet sufficiently informative evaluations was introduced to overcome the difficulties discussed above. The method consisted of heating a specimen from 600 to 1685°C at a constant rate of 10°C/minute while it was suspended in the induction-radiation setup. After the maximum temperature was reached, the furnace power was turned off but the sample was left in the furnace until it cooled down to 800°C. During the complete heating and cooling cycle, the weight changes were recorded as a function of time. This procedure has the following advantages over isothermal testing:

1) All temperatures are equally evaluated. There are no temperature gaps and, consequently, no chances of missing a critical oxidation temperature within the given range.

2) The effectiveness of a coating formed at a higher temperature can be checked at lower temperatures as the specimen is cooled.

3) A plot of the oxidation rate as a function of temperature pinpoints temperature regions where coatings are formed as well as regions where the protection afforded is insufficient.

4) Under these conditions of oxidation, most of the composites in question begin to form protective coatings at relatively low

temperatures. Since the platinum suspension wire is not in direct contact with unoxidized ingredients when approaching higher temperatures, no alloying takes place and the melting point of the wire is not lowered. In case of isothermal testing, the platinum wire alloyed with ingredients of the composite and melted at temperatures as low as 1400°C thus ruling out the use of the induction-radiation setup for measurements at higher temperatures.

The apparent disadvantage of the dynamic test is that it does not provide any information on the change of the oxidation rate at a certain temperature as a function of time. Oxidation rates of graphite base composites, however, generally decrease with time so that the dynamic test may be considered realistic inasmuch as it reflects the adverse starting characteristics of isothermal oxidation curves.

Dynamic-oxidation characteristics for the JTA composite are illustrated in Figures 32 and 33 where weight loss and oxidation rate are plotted as a function of temperature. A relatively high weight

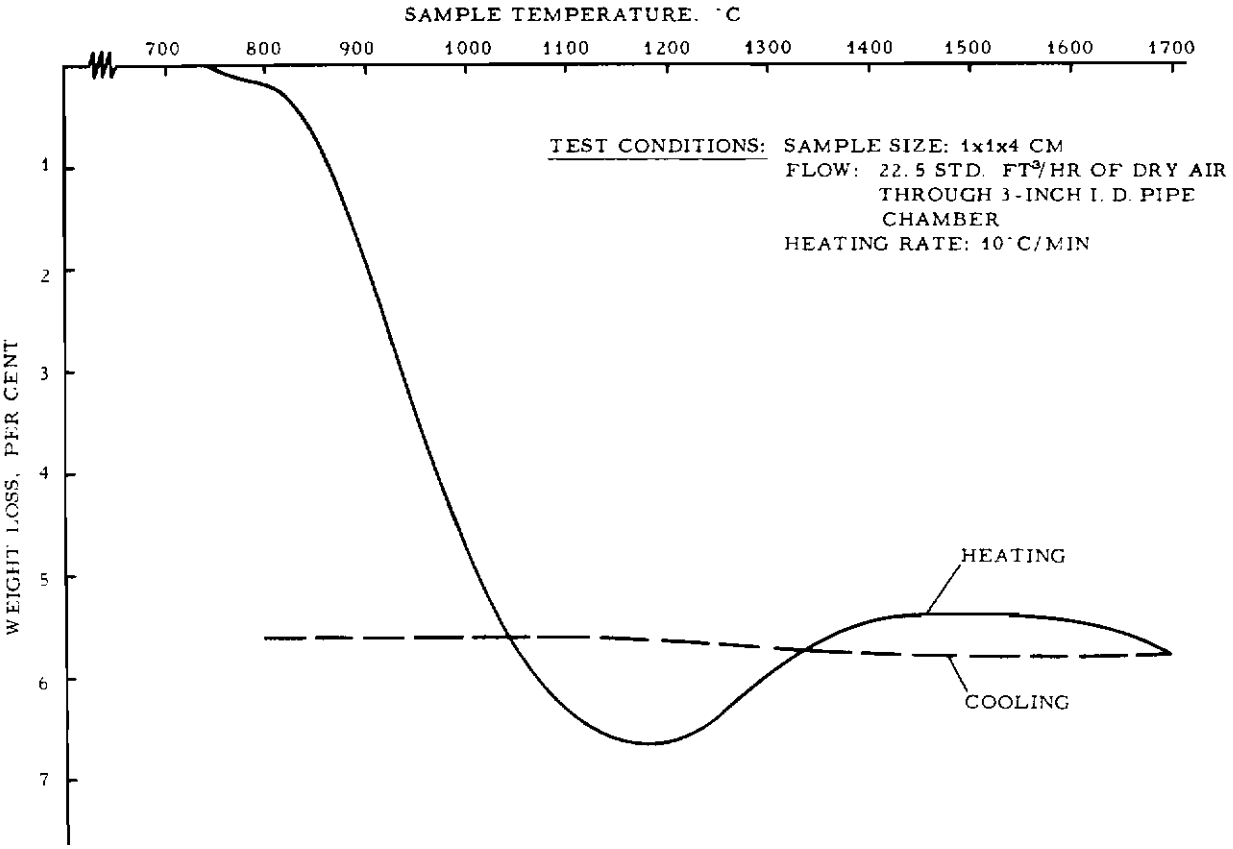

Figure 32. Dynamic Oxidation Characteristic of JTA, Weight Loss versus Temperature

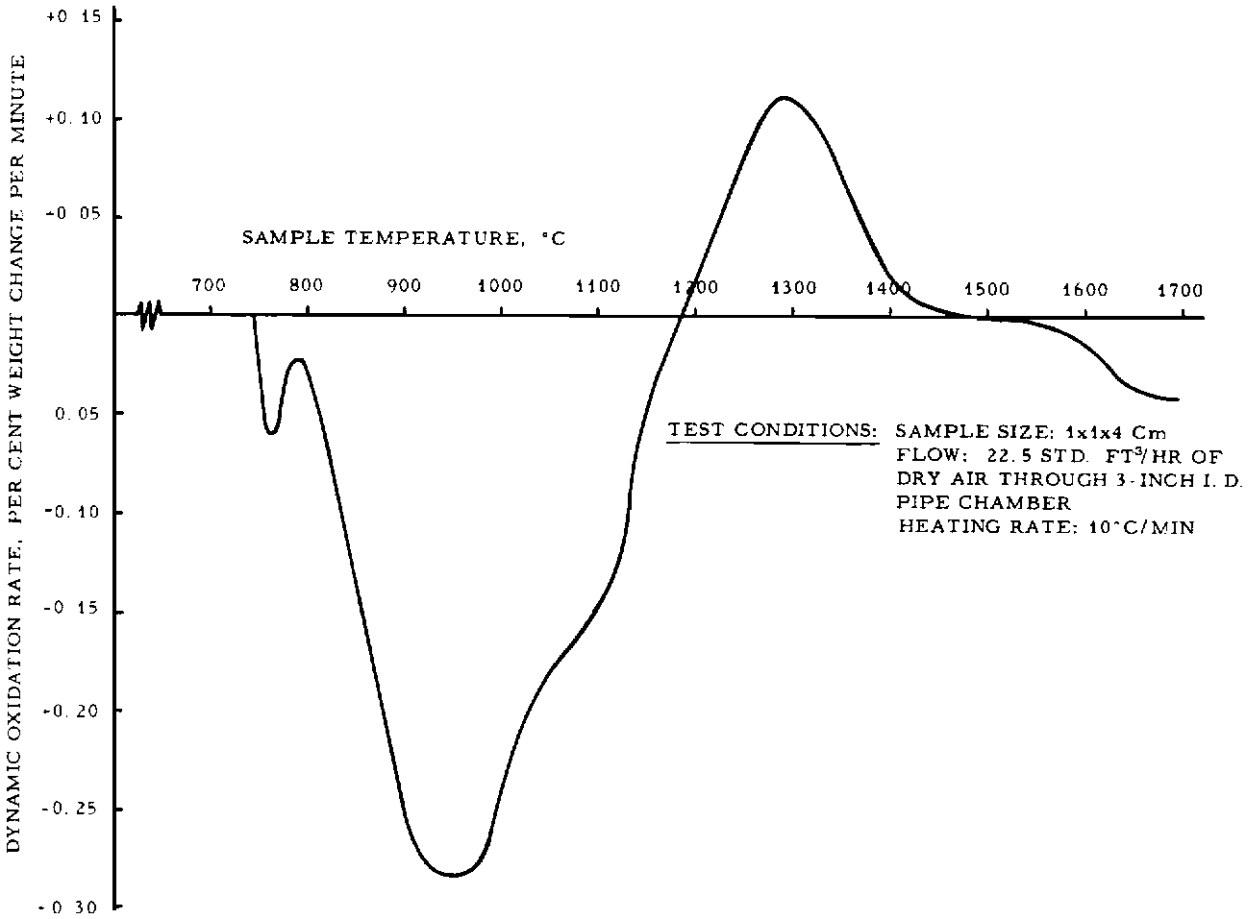

Figure 33. Dynamic Oxidation Characteristic of JTA, Oxidation Rate versus Temperature

loss occurred over the temperature range of 850 to 1100°C while the material gained weight when heated from 1200 to 1450°C, indicating the rapid buildup of a coating during the latter temperature interval.

A series of investigations was made in an attempt to close the gap in the protective mechanism at the lower temperature range. This was done by successive modifications of the JTA composite wherein various amounts of its additives were replaced by others. Figure 34 shows what happens when increasing percentages of the ZrB_2 content were replaced by elemental boron. The low temperature oxidation resistance was greatly improved with rising boron content, and a high enough amount of this additive completely eliminated the described nonprotective gap. On the other hand, the best low temperature oxidation resistance obtained in this manner was accompanied by a diminished high temperature oxidation resistance as evidenced by the increased slope of the curve at the maximum temperature of the test cycle. Also, a reduced coating stability was indicated by the continuing weight loss during the major part of the cooling period.

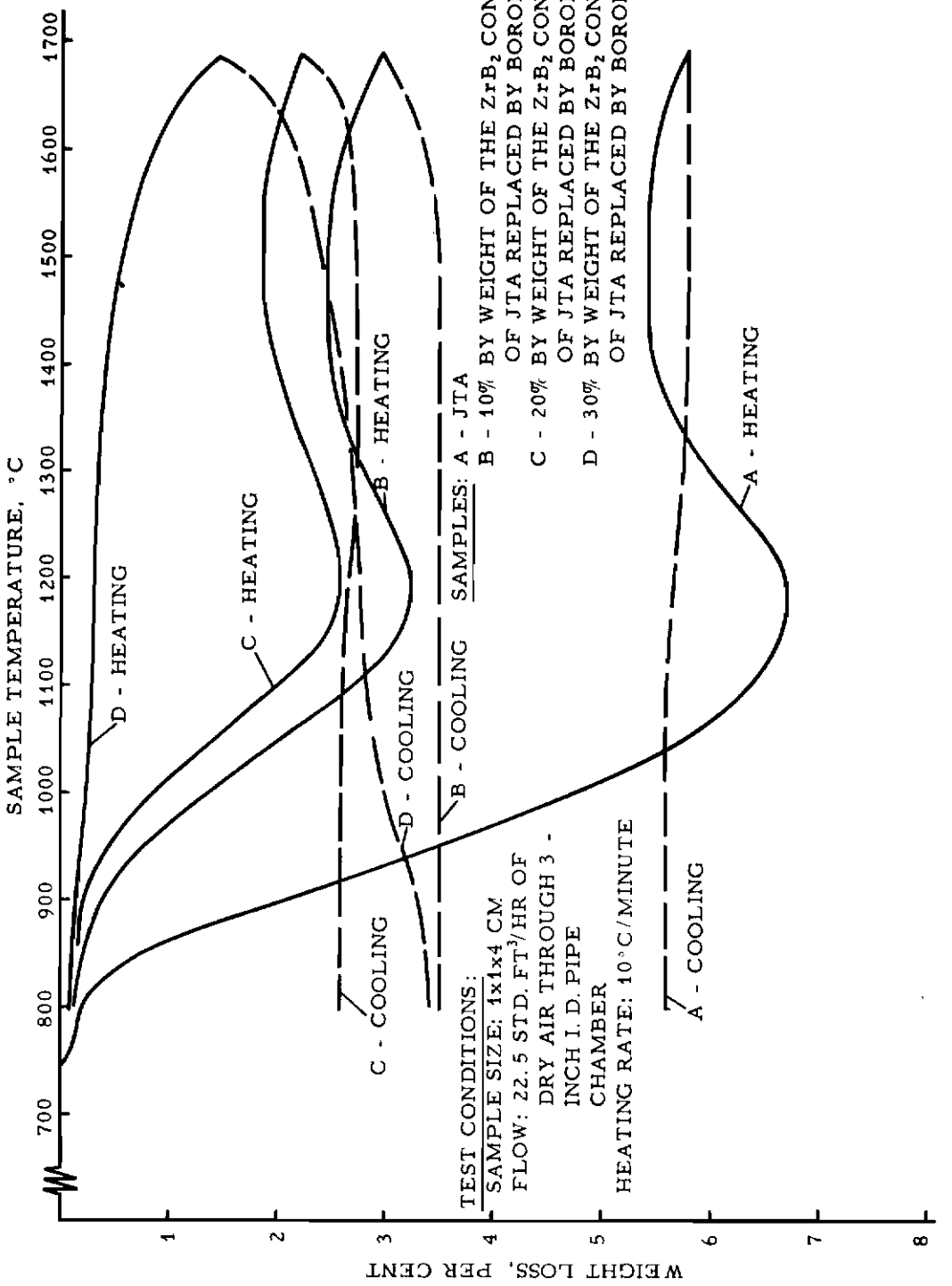

Figure 34. Effect of Boron Replacing ZrB_2 in JTA, Demonstrated by Dynamic Oxidation Characteristics

Similar effects were observed for other additives. Figure 35 illustrates the effect of hafnium, columbium, and titanium diboride when substituted for some of the ZrB_2 content of the material characterized by curve B in Figure 34. Considering the enlarged scale of Figure 35 as compared with Figure 34, it is seen that Hf, Cb, and

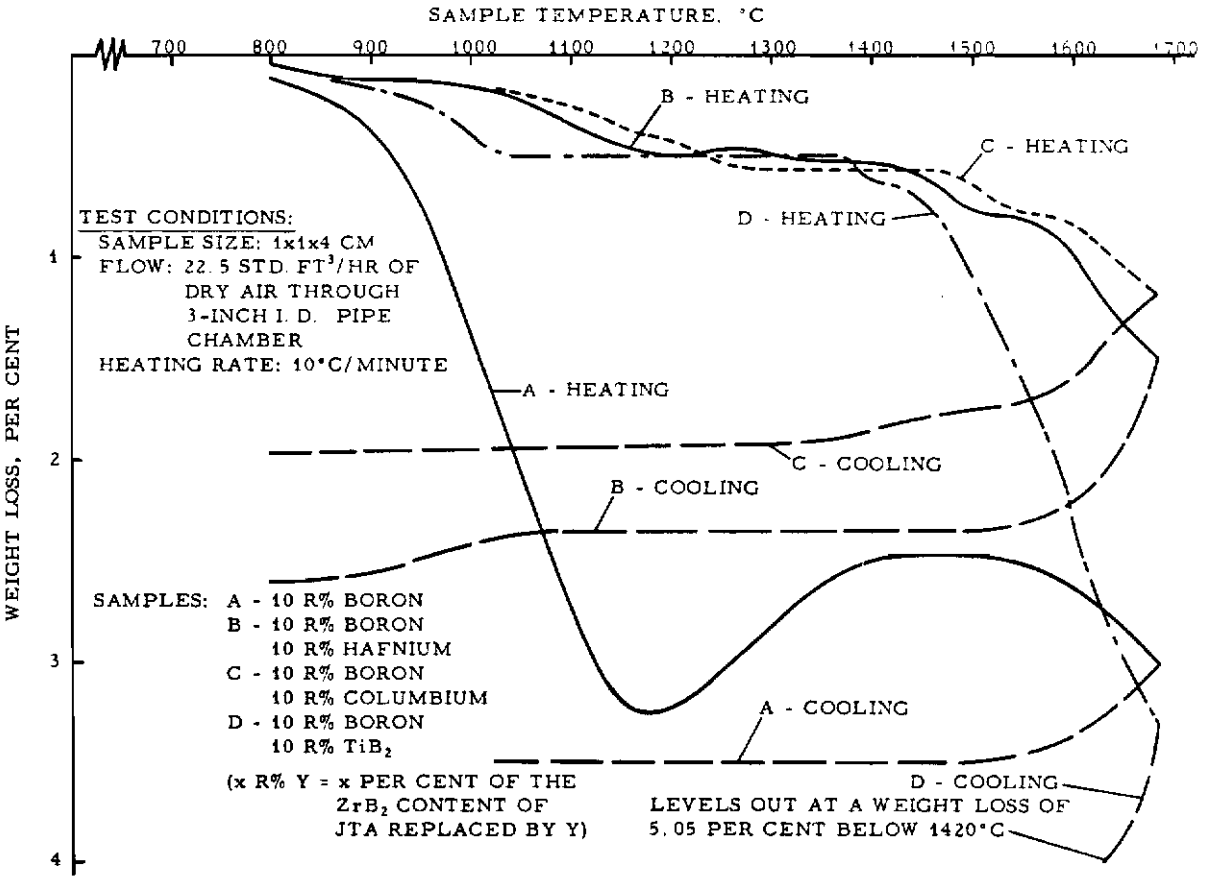

Figure 35. Effect of Hafnium, Columbium, and TiB_2 Replacing ZrB_2 in Boronated JTA, Demonstrated by Dynamic Oxidation Characteristics

TiB_2 increased the low temperature oxidation resistance more effectively than an equal amount of boron (curve C in Figure 34) but that TiB_2 had to be ruled out because of very poor performance at higher temperatures. The latter point is emphasized in Figure 36 which shows the appearance of relevant samples after dynamic-oxidation testing. In all of the specimens shown in Figure 36, 20 per cent of the ZrB_2 in the JTA composite was replaced by other additives with at least one-half of the replacement being boron. It can be seen in this figure that the coating formed by the specimen containing TiB_2 was molten while no such evidence existed for the other specimens. The free boron seemed to enhance the melting of the coating in question but was not solely responsible for the phenomenon.

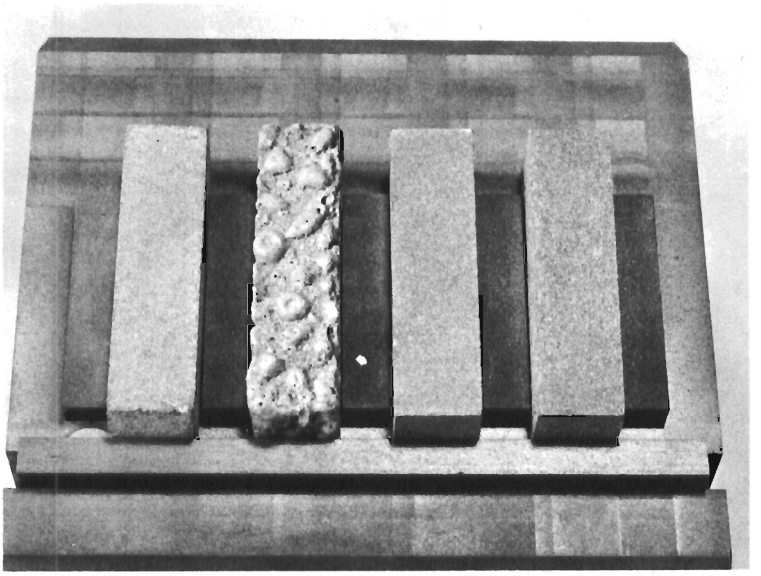

Compositional Difference from Left to Right:

1) 20 R% Boron
2) 10 R% Boron
   10 R% TiB_2
3) 10 R% Boron
   10 R% Hafnium
4) 10 R% Boron
   10 R% Columbium

XR% Y = X per cent by weight of ZrB_2 content of JTA replaced by Y

Figure 36. Appearance of Samples after Dynamic Oxidation Test, Effect of Hafnium, Columbium, and TiB_2 Replacing Boron in Boronated JTA

This is illustrated in Figure 37 where the JTA composite is compared, after the dynamic-oxidation cycle, with samples in which 10 per cent of the ZrB_2 content was replaced by boron, titanium diboride, and hafnium, respectively. Once more, the sample containing TiB_2 is the only one which exhibited obvious melting of the coating although the viscosity of the melt appeared to be higher than in the corresponding case of Figure 36.

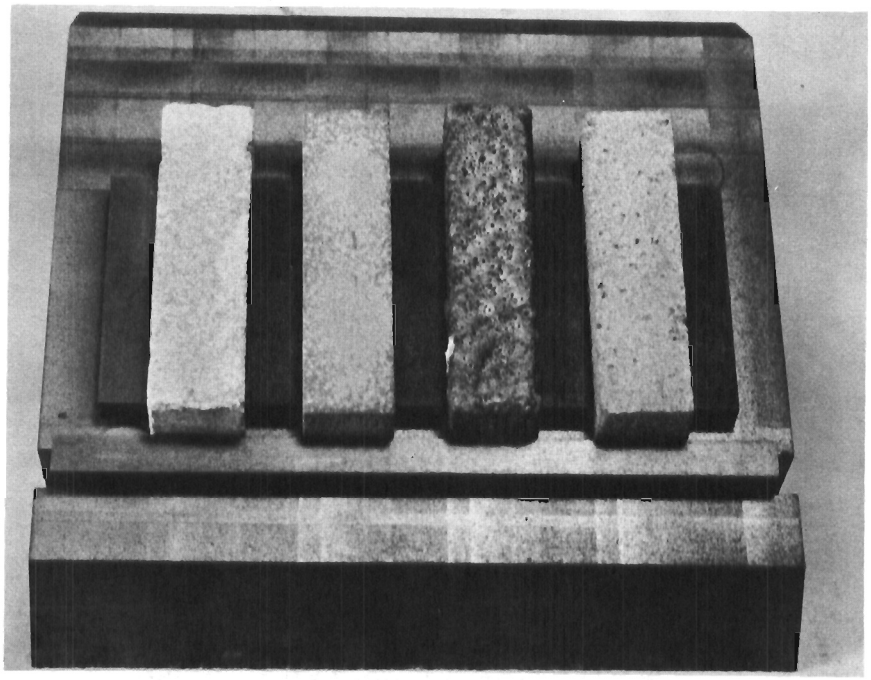

Compositional Difference from Left to Right:

1) Standard JTA
2) 10 R% Boron
3) 10 R% TiB_2
4) 10 R% Hafnium

XR% Y = X per cent by weight of ZrB_2 content of JTA replaced by Y

Figure 37. Appearance of Samples after Dynamic Oxidation Test, Effect of Boron, TiB_2, and Hafnium Replacing ZrB_2 in JTA

The good results obtained with boron and columbium, as illustrated in Figure 34, led to investigations in which increasing amounts of ZrB_2 were replaced with Cb. The results, shown in Figure 38, indicated that this was not beneficial.

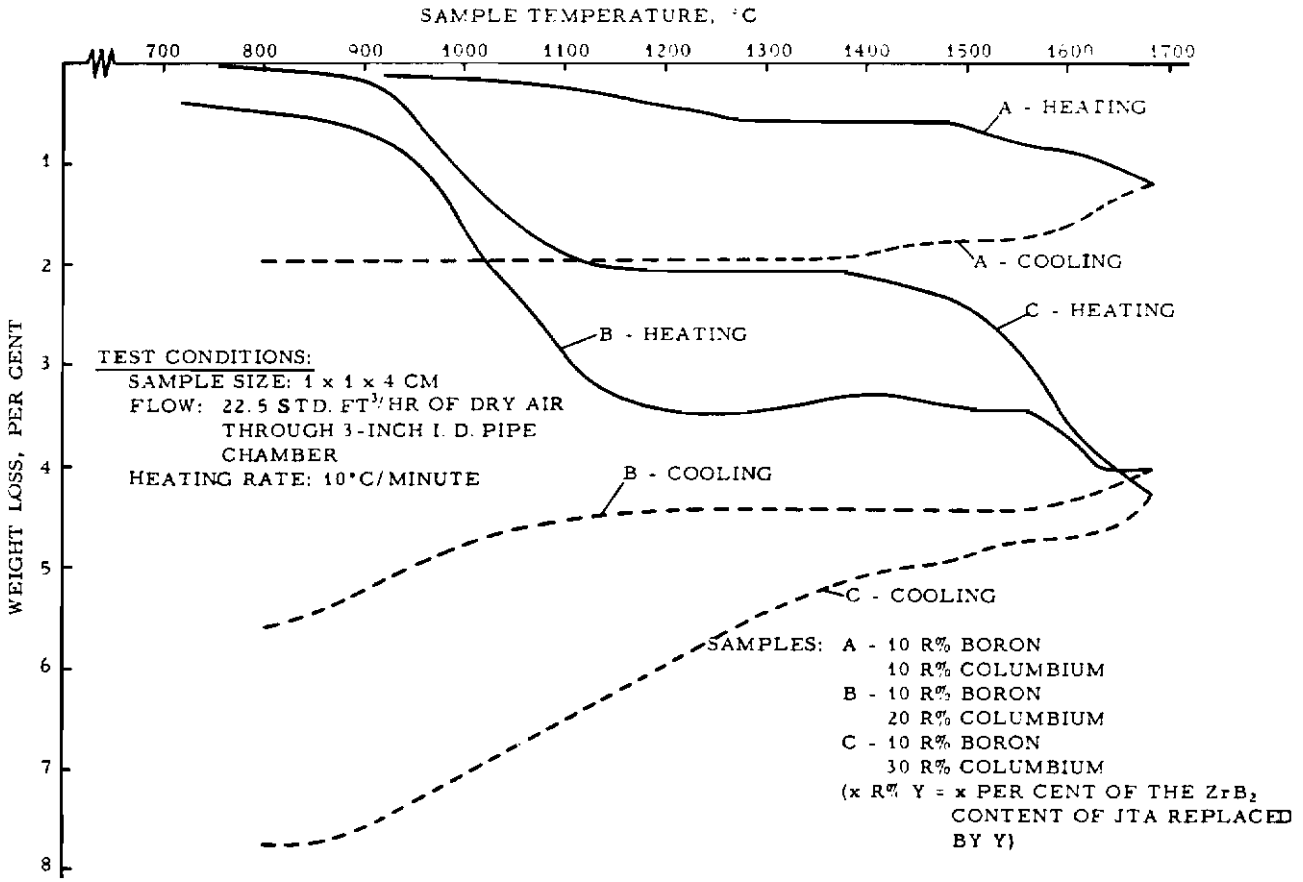

Figure 38. Effect of Columbium Replacing ZrB_2 in Boronated JTA, Demonstrated by Dynamic Oxidation Characteristics

A similar investigation was carried out for CrB_2. The findings, as given in Figure 39, indicated a good protective mechanism in the lower temperature range but extremely poor performance at higher temperatures. After the given oxidation cycle, these samples exhibited extensive melting of the coating as well as the formation of large globules, very similar to the specimen containing TiB_2 in Figure 36.

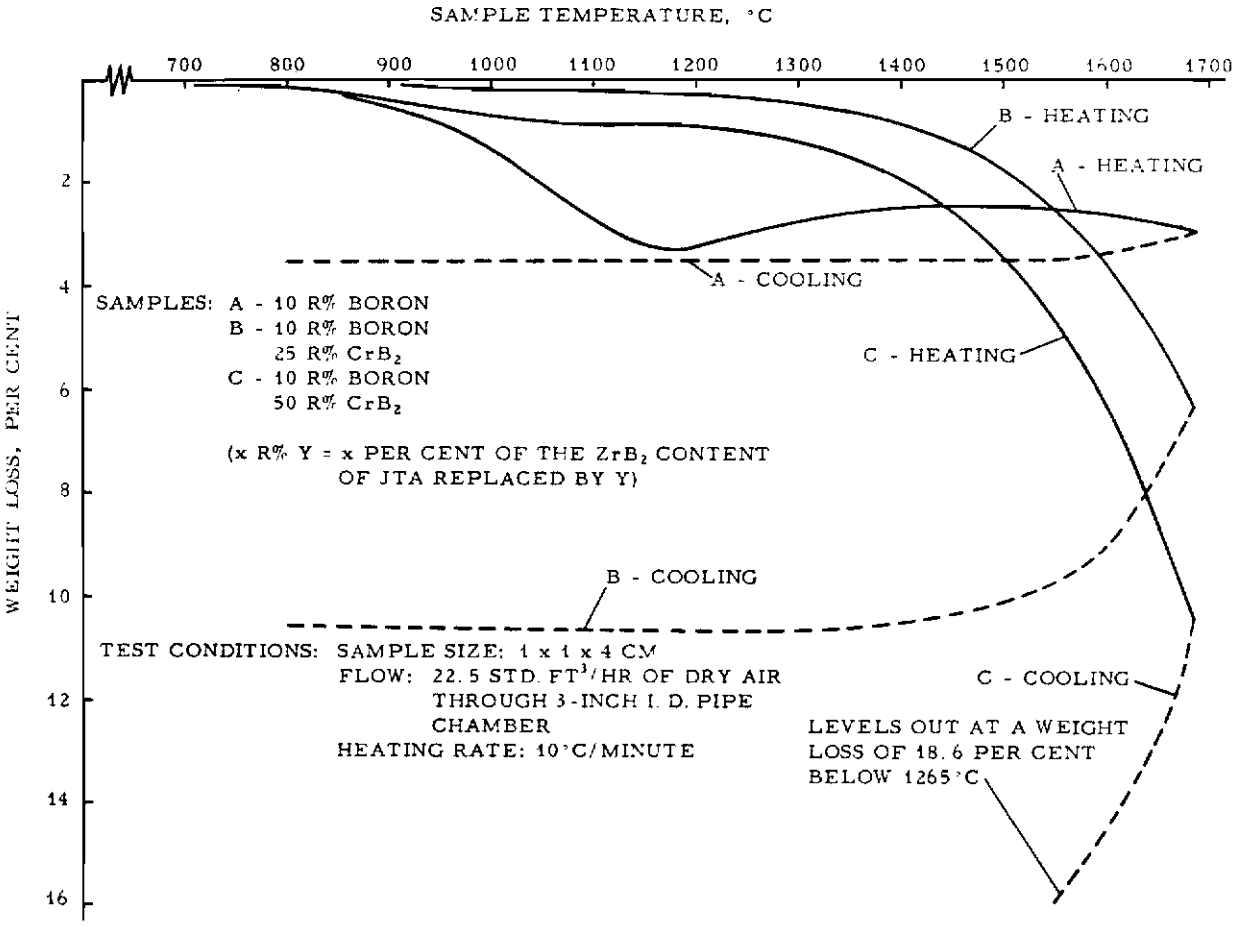

Figure 39. Effect of CrB_2 Replacing ZrB_2 in Boronated JTA, Demonstrated by Dynamic Oxidation Characteristics

The next series of experiments involved replacing varying amounts of the ZrB_2 in the JTA composite with thorium while a constant amount of the ZrB_2 was replaced with boron. Thorium was attractive as an additive because its oxide is very stable and has the highest melting point of all oxides. Figure 40 shows the results of the oxidation tests when various amounts of the zirconium diboride content of the JTA composite are replaced by thorium while a constant amount is replaced by boron. These results show that only small amounts of thorium were beneficial in the C/ZrB_2/B/Th/Si system at the given temperature range.

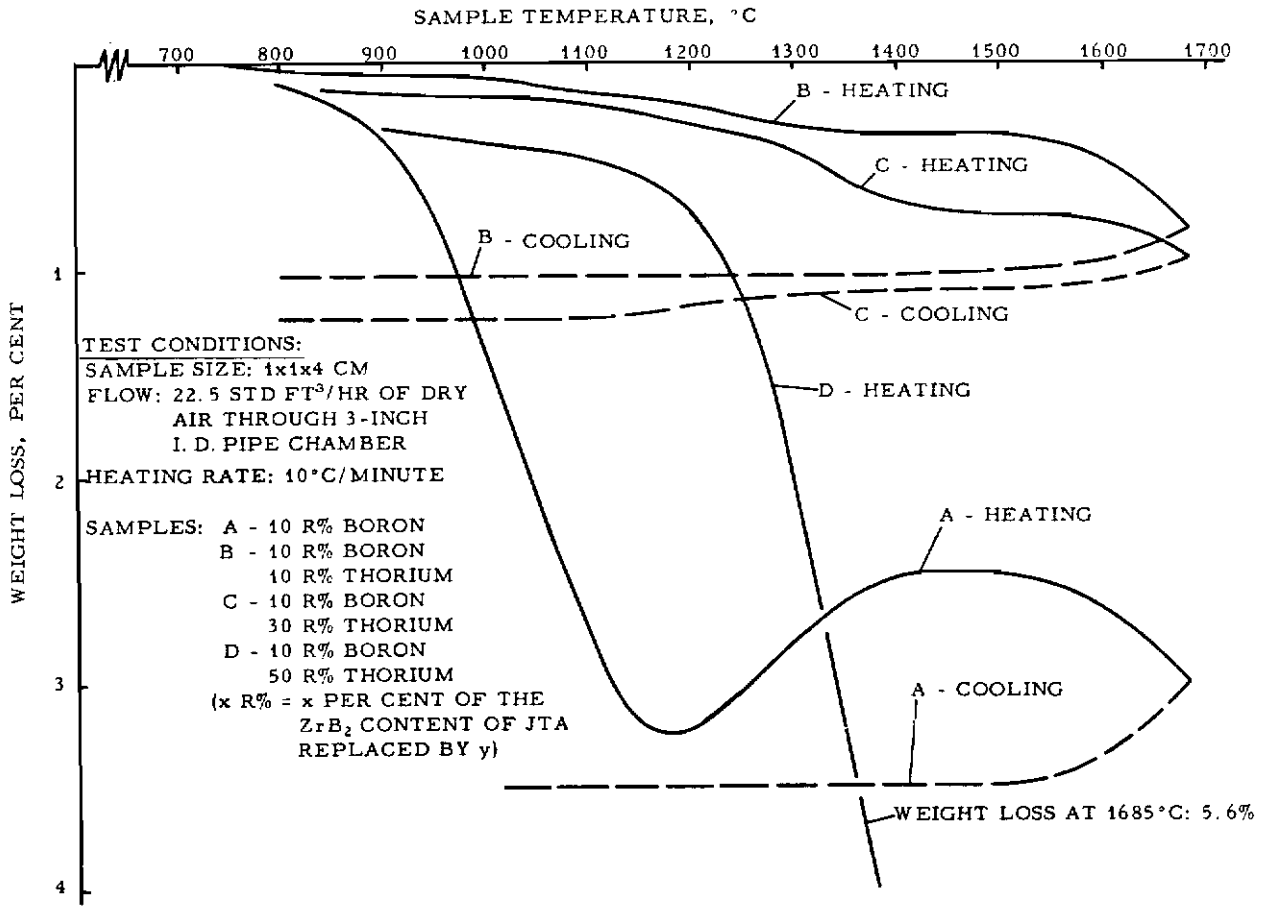

Figure 40. Effect of Thorium Replacing ZrB_2 in Boronated JTA, Demonstrated by Dynamic Oxidation Characteristics

A different basic picture was obtained for other combinations. Figure 41 shows, on an enlarged scale, the changes effected when thorium was used to replace various amounts of the Si content of the material characterized by curve C in Figure 35 which was an excellent performer. While the total weight loss of the thoriated grades at the maximum temperature of the test cycle was about equal to that of the $C/ZrB_2/B/Cb/Si$ system, the exchange from silicon to thorium produced a positive oxidation rate (weight gain) at this top test temperature. Of the many composites investigated, these were the first ones to exhibit stability at temperatures in excess of the maximum temperature of the given test.

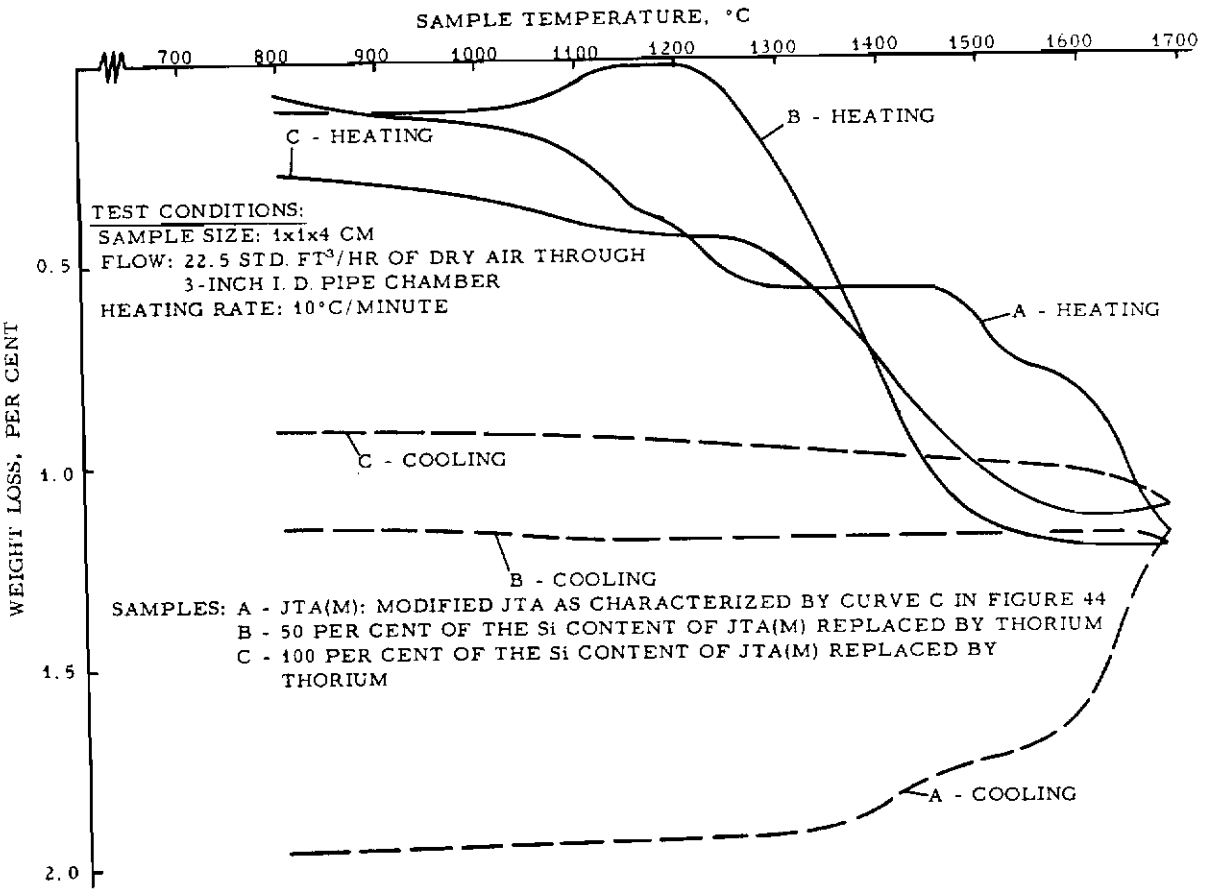

Figure 41. Effect of Thorium Replacing Silicon in Modified JTA, Demonstrated by Dynamic Oxidation Characteristics

Similarly favorable results were obtained with the replacement of silicon (curve C, Figure 35) by boron, and these results are illustrated in Figure 42. Attention is drawn again to the enlarged scale of the graph as compared with previous presentations. The composite represented here by curve C was the first one to exhibit an overall weight gain after the cycle, and the weight losses during the cycle were so small as to be within the error of measurement.

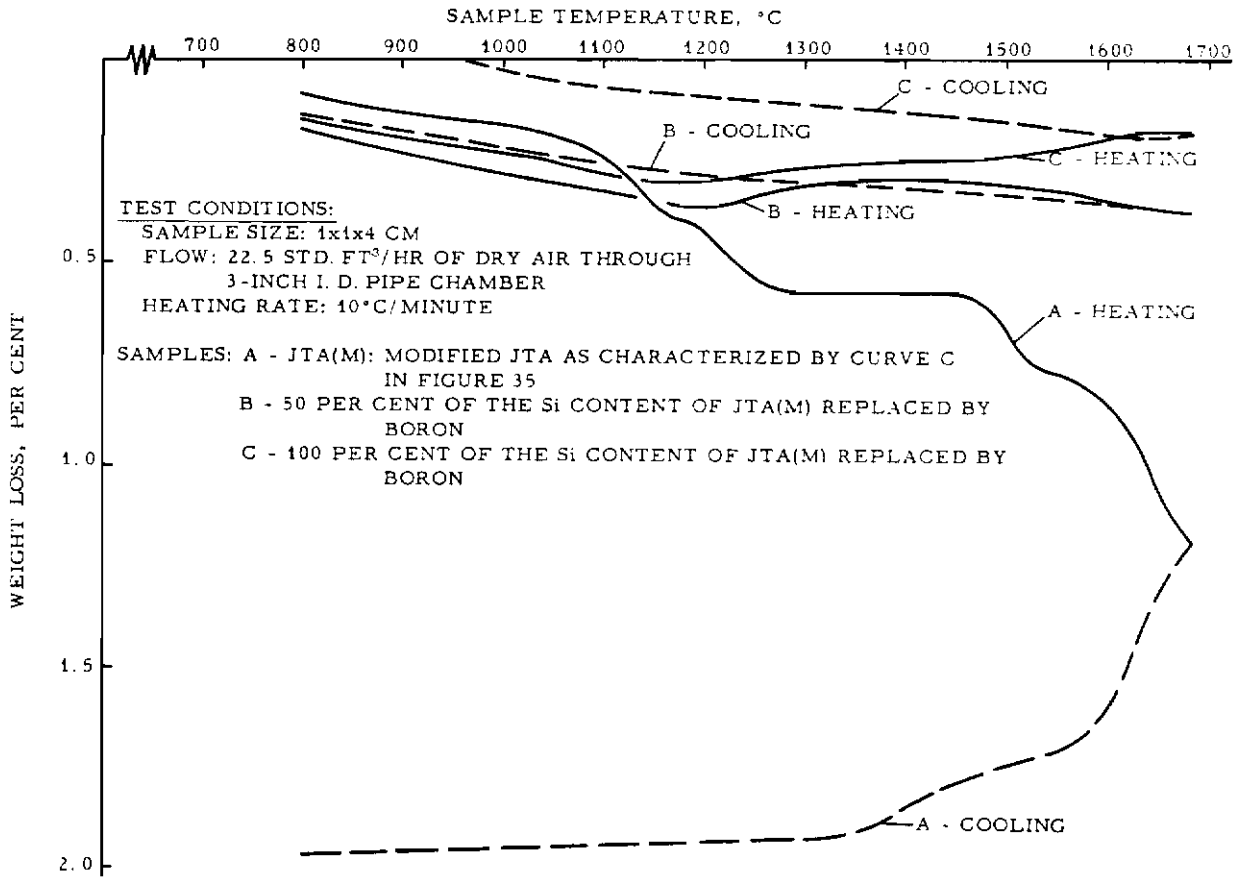

Figure 42. Effect of Boron Replacing Silicon in Modified JTA, Demonstrated by Dynamic Oxidation Characteristics

The appearance of the specimens, represented by the curves B and C in both Figures 41 and 42, after the given test cycle is illustrated in Figure 43. All of these very effective coatings look quite inconspicuous and none of them exhibits any sign of melting. On the other hand, as a reminder of the severity of the test, an ATJ sample of the same size completely oxidized and disintegrated before reaching the maximum temperature of the test cycle.

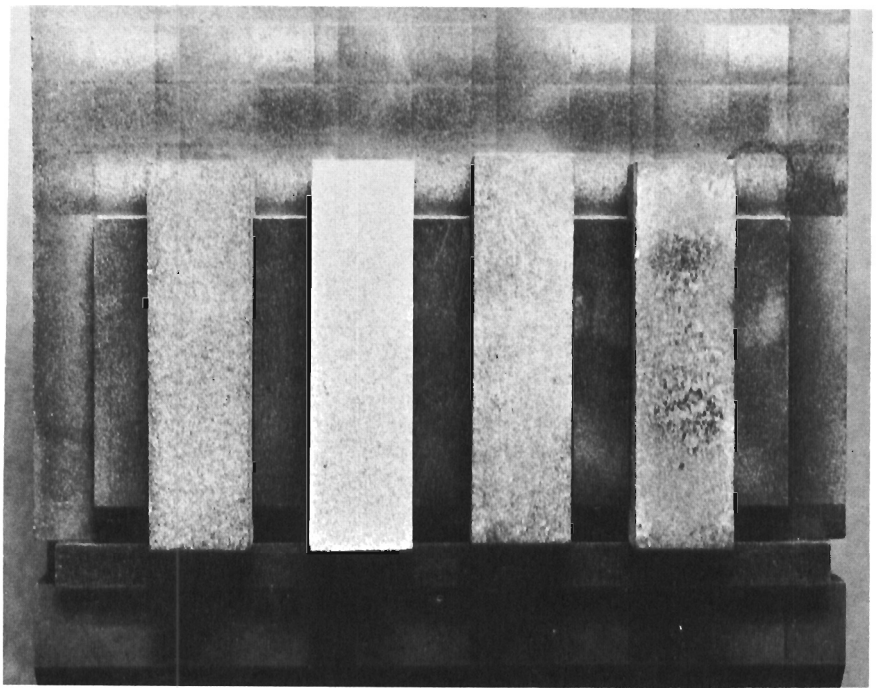

Compositional Difference from Left to Right:

1) 50 Q per cent thorium
2) 100 A per cent thorium
3) 50 Q per cent boron
4) 100 A per cent boron

(XQ per cent Y = X per cent by weight of the Si content of the reference grade replaced by Y, the reference grade being a JTA modification wherein 10 per cent by weight of the ZrB_2 content of JTA were replaced by B and 10 analagous per cent by Cb)

Figure 43. Appearance of Samples after Dynamic Oxidation Test, Effect of Thorium and Boron Replacing Silicon in Modified JTA

The composite represented by curve C in Figure 42 has been submitted to additional isothermal testing at various temperatures to establish its oxidation rate as a function of time and to check the conclusions drawn from the dynamic oxidation test. Results, compiled in Table 1, confirmed the value of the dynamic oxidation procedure. Weight changes were less than one-half of one per cent for this composite at all test temperatures for 200-minute exposures. The problem of providing a graphite base material with essentially permanent oxidation resistance at low and intermediate temperatures has been solved with this $C/ZrB_2/B/Cb$ composite. The success with this composite also shows that achievement of permanent oxidation protection by composite technology is feasible. Since the principle has been demonstrated for moderately high temperatures, it should be possible to provide oxidation protection at very high temperatures with the proper selection and combination of additives.

Table 1. Isothermal Oxidation Characteristics of an Advanced Composite

Composition before Processing:		73 per cent by weight graphite 27 per cent by weight 175°C pitch 66 PPH* ZrB_2 8.25 PPH columbium 26.75 PPH boron				
Test Conditions:	Sample Size -	1 by 1 by 4 cm				
	Air Flow -	22.5 std. ft^3/hr through 3-inch ID pipe chamber				
Temperature in °C		800	1100	1400	1600	1660
Weight change in per cent after 200 minutes		-0.16	+0.04	+0.08	-0.09	-0.38
Maximum weight change in per cent during 200 minutes		-0.26	-0.12	+0.17	-0.13	-0.38

* PPH = parts per hundred parts of carbonaceous base material, by weight

6. SUMMARY OF COMPOSITIONS INVESTIGATED

All compositions investigated have been compiled in Table 2. Each entry gives the processing conditions as well as a number of the principal properties of the resulting product. The following abbreviations are used in Table 2:

W - per cent by weight

PPH - parts per hundred parts of carbonaceous base material on a weight basis

$\varkappa\Big|_{o}^{x}(y)$ - mean specific oxidation rate during the first x minutes of exposure at y°C as measured in the induction-radiation setup in a flow of 22.5 std. ft^3/hr of dry air through a 3-inch ID pipe chamber

$\beta\Big|_{x}^{y}$ - dynamic oxidation characteristic at a heating rate of 10°C/h between x°C and y°C as measured in the induction-radiation setup in a flow of 22.5 std. ft^3/hr of dry air through a 3-inch ID pipe chamber

S(y) - flexural strength at y°C as determined under the following test conditions:

sample size: 1 by 1 by 4 cm
span: 1 1/4 inches
3-point loading
load rate: 1 lb/second

$\rho(y)$ - electrical resistivity at y°C

$\lambda(y)$ - thermal conductivity at y°C

CTE(y) - coefficient of thermal expansion at y°C

A.G. - across-the-grain direction

W.G. - with (parallel to) -the-grain direction

R.T. - room temperature

B.D. - bulk density

PSI - pounds per square inch

Table 2. The Compositions Investigated and Principal Properties of the Resulting Products

No.	Compositions	Processing Conditions Employed	Characteristics
1	81.5 W% Coke Flour 18.5 W% B_4C	5000 PSI from R. T. to 2250°C	B. D. = 2.17 g/cc S(25) A. G. = 4,070 PSI ρ(25) A. G. = 15.3 x 10^{-4} OHM cm
2	90.65 W% Coke Flour 9.35 W% B_4C	5000 PSI from R. T. to 2550°C	B. D. = 2.17 g/cc S(25) A. G. = 3,280 PSI ρ (25) A. G. = 13.6 x 10^{-4} OHM cm
3	80 W% Coke Flour 20 W% 175°C Pitch 20 PPH B_4C	2500 PSI from R. T. to 2000°C 6250 PSI from 2000°C to 3000°C	B. D. = 2.13 g/cc S(25) W. G. = 9,800 PSI ρ (25) W. G. = 3.9 x 10^{-4} OHM cm $\kappa\Big\|_0^{10}$ (800) = - 11 mg/cm²h
4	80 W% Coke Flour 20 W% 175°C Pitch 40 PPH Hf	2500 PSI from R. T. to 2200°C 6250 PSI from 2200°C to 3000°C	B. D. = 2.93 g/cc S(25) W. G. = 5,610 PSI ρ (25) W. G. = 3.7 x 10^{-4} OHM cm $\kappa\Big\|_0^{10}$ (800) = - 222 mg/cm²h
5	80 W% Coke Flour 20 W% 175°C Pitch 40 PPH Ta	2500 PSI from R. T. to 2600°C 6250 PSI from 2600°C to 3100°C	B. D. = 2.90 g/cc S(25) W. G. = 6,290 PSI ρ (25) W. G. = 2.5 x 10^{-4} OHM cm $\kappa\Big\|_0^{10}$ (800) = -190 mg/cm²h
6	80 W% Coke Flour 20 W% 175°C Pitch 40 PPH Cb	2500 PSI from R. T. to 2200°C 6250 PSI from 2200°C to 3000°C	B. D. = 2.80 g/cc S(25) W. G. = 6,070 PSI ρ (25) W. G. = 3.0 x 10^{-4} OHM cm $\kappa\Big\|_0^{10}$ (800) = -155 mg/cm²h
7	90 W% Coke Flour 10 W% ZrC	2250 PSI from R. T. to 2600°C 5750 PSI from 2600°C to 3100°C	B. D. = 2.25 g/cc S(25) W. G. = 6,500 PSI S(25) A. G. = 1,760 PSI ρ (25) W. G. = 1.7 x 10^{-4} OHM cm ρ (25) A. G. = 13.6 x 10^{-4} OHM cm
8	75 W% Coke Flour 25 W% ZrC	2250 PSI from R. T. to 2600°C 5750 PSI from 2600°C to 3100°C	B. D. = 2.31 g/cc S(25) W. G. = 7,650 PSI S(25) A. G. = 2,415 PSI ρ (25) W. G. = 1.6 x 10^{-4} OHM cm ρ (25) A. G. = 8.7 x 10^{-4} OHM cm

Table 2, Continued

No.	Compositions	Processing Conditions Employed	Characteristics
9	80 W% Coke Flour 20 W% 175°C Pitch 10 PPH ZrC	2250 PSI from R. T. to 2600°C 5750 PSI from 2600°C to 3100°C	B. D. = 2.23 g/cc S(25) W. G. = 5,200 PSI S(25) A. G. = 1,800 PSI ρ (25) W. G. = 3.0×10^{-4} OHM cm ρ (25) A. G. = 12.9×10^{-4} OHM cm
10	80 W% Coke Flour 20 W% 175°C Pitch 20 PPH ZrC	2250 PSI from R. T. to 2600°C 5750 PSI from 2600°C to 3100°C	B. D. = 2.26 g/cc S(25) W. G. = 8,350 PSI S(25) A. G. = 2,520 PSI ρ (25) W. G. = 2.3×10^{-4} OHM cm ρ (25) A. G. = 9.5×10^{-4} OHM cm
11	80 W% Coke Flour 20 W% 175°C Pitch 30 PPH ZrC	2250 PSI from R. T. to 2600°C 5750 PSI from 2600°C to 3100°C	B. D. = 2.31 g/cc S(25) W. G. = 8,920 PSI S(25) A. G. = 3,110 PSI ρ (25) W. G. = 1.9×10^{-4} OHM cm ρ (25) A. G. = 7.3×10^{-4} OHM cm
12	80 W% Coke Flour 20 W% 175°C Pitch 40 PPH ZrC	2250 PSI from R. T. to 2600°C 5750 PSI from 2600°C to 3100°C	B. D. = 2.33 g/cc S(y) W. G. and A. G. see Fig. 15 $\kappa\Big|_0^{10}$ (800) = -200 mg/cm^{2}h
13	80 W% Coke Flour 20 W% 175°C Pitch 5 PPH TiB_2	2500 PSI from R. T. to 2400°C 6250 PSI from 2400°C to 2800°C	B. D. = 2.18 g/cc S(25) W. G. = 9,420 PSI ρ (25) W. G. = 3.2×10^{-4} OHM cm $\kappa\Big|_0^{10}$ (800) = -42 mg/cm^{2}h
14	80 W% Coke Flour 20 W% 175°C Pitch 10 PPH TiB_2	2500 PSI from R. T. to 2400°C 6250 PSI from 2400°C to 2800°C	B. D. = 2.19 g/cc S(y) W. G. and A. G. see Fig. 14 $\kappa\Big|_0^{10}$ (800) = -15 mg/cm^{2}h CTE(200) W. G. = 1.8×10^{-6}/°C CTE(200) A. G. = 8.8×10^{-6}/°C ρ (25) W. G. = 2.4×10^{-4} OHM cm ρ (25) A. G. = 8.3×10^{-4} OHM cm
15	80 W% Coke Flour 20 W% 175°C Pitch 15 PPH TiB_2	2500 PSI from R. T. to 2400°C 6250 PSI from 2400°C to 2800°C	B. D. = 2.18 g/cc S(25) W. G. = 11,310 PSI $\kappa\Big|_0^{10}$ (800)= -12.5 mg/cm^{2}h
16	80 W% Coke Flour 20 W% 175°C Pitch 20 PPH TiB_2	2500 PSI from R. T. to 2400°C 6250 PSI from 2400°C to 2800°C	B. D. = 2.18 g/cc S(25) W. G. = 11,800 PSI $\kappa\Big|_0^{10}$ (800) = -11 mg/cm^{2}h

Table 2, Continued

No.	Compositions	Processing Conditions Employed	Characteristics
17	80 W% Coke Flour 20 W% 175°C Pitch 40 PPH TiB_2	2500 PSI from R. T. to 2400°C 6250 PSI from 2400°C to 2800°C	B. D. = 2.19 g/cc S(25) W. G. = 11,900 PSI $\kappa\Big\|_0^{10}$ (800) = -11 mg/cm²h
18	80 W% Coke Flour 20 W% 175°C Pitch 10 PPH Si	2500 PSI from R. T. to 2200°C 6250 PSI from 2200°C to 2650°C	B. D. = 2.07 g/cc S(25) W. G. = 4,870 PSI ρ (25) W. G. = 6.8×10^{-4} OHM cm $\kappa\Big\|_0^{10}$ (800) = -190 mg/cm²h
19	80 W% Coke Flour 20 W% 175°C Pitch 20 PPH Si	2500 PSI from R. T. to 2200°C 6250 PSI from 2200°C to 2650°C	B. D. = 2.16 g/cc S(25) W. G. = 4,960 PSI ρ (25) W. G. = 8.8×10^{-4} OHM cm $\kappa\Big\|_0^{10}$ (800) = -149 mg/cm²h
20	80 W% Coke Flour 20 W% 175°C Pitch 10 PPH $MoSi_2$	2500 PSI from R. T. to 1800°C	B. D. = 1.79 g/cc S(25) W. G. = 2,900 PSI $\kappa\Big\|_0^{30}$ (1200) = -432 mg/cm²h
21	80 W% Coke Flour 20 W% 175°C Pitch 20 PPH $MoSi_2$	2500 PSI from R. T. to 1800°C	B. D. = 1.82 g/cc $\kappa\Big\|_0^{30}$ (1200) = -390 mg/cm²h
22	80 W% Coke Flour 20 W% 175°C Pitch 30 PPH $MoSi_2$	2500 PSI from R. T. to 1800°C	B. D. = 1.95 g/cc $\kappa\Big\|_0^{30}$ (1200)= -316 mg/cm²h
23	80 W% Coke Flour 20 W% 175°C Pitch 40 PPH $MoSi_2$	2500 PSI from R. T. to 1800°C 6250 PSI from 1800°C to 2800°C	B. D. = 2.24 g/cc S(25) W. G. = 10,380 PSI ρ(25) W. G. = 3.4×10^{-4} OHM cm $\kappa\Big\|_0^{10}$ (800) = -193 mg/cm²h
24	80 W% Coke Flour 20 W% 175°C Pitch 2.5 PPH TiB_2 2.5 PPH B_4C	2550 PSI from R. T. to 2400°C 6350 PSI from 2400°C to 2800°C	B. D. = 2.05 g/cc S(25) W. G. = 9,800 PSI $\kappa\Big\|_0^{10}$ (800) = -35 mg/cm²h

Table 2, Continued

No.	Compositions	Processing Conditions Employed	Characteristics
25	80 W% Coke Flour 20 W% 175°C Pitch 5 PPH TiB_2 5 PPH B_4C	2550 PSI from R. T. to 2400°C 6350 PSI from 2400°C to 2800°C	B. D. = 2.36 g/cc S(25) W. G. = 10,300 PSI $\kappa\Big|_0^{10}$ (800) = -30 mg/cm²h
26	80 W% Coke Flour 20 W% 175°C Pitch 7.5 PPH TiB_2 7.5 PPH B_4C	2550 PSI from R. T. to 2400°C 6350 PSI from 2400°C to 2800°C	B. D. = 2.58 g/cc S(25) W. G. = 10,500 PSI $\kappa\Big|_0^{10}$ (800) = -25 mg/cm²h
27	80 W% Coke Flour 20 W% 175°C Pitch 6.5 PPH B_4C 3.5 PPH Si	2500 PSI from R. T. to 2000°C 6250 PSI from 2000°C to 2650°C	$\kappa\Big|_0^{10}$ (800) = -16.5 mg/cm²h
28	80 W% Coke Flour 20 W% 175°C Pitch 13 PPH B_4C 7 PPH Si	2500 PSI from R. T. to 2000°C 6250 PSI from 2000°C to 2650°C	S(25) W. G. = 12,200 PSI S(1500) W. G. = 15,800 PSI S(25) A. G. = 5,100 PSI S(1500) A. G. = 6,500 PSI CTE(200) W. G. = 1.4×10^{-6}/°C CTE(200) A. G. = 5.4×10^{-6}/°C $\kappa\Big|_0^{10}$ (800) = -9.7 mg/cm²h $\kappa\Big|_0^{x}$ (1200) see Fig. 18
29	80 W% Coke Flour 20 W% 175°C Pitch 19.5 PPH B_4C 10.5 PPH Si	2500 PSI from R. T. to 2000°C 6250 PSI from 2000°C to 2650°C	S(25) W. G. = 13,800 PSI $\kappa\Big|_0^{10}$ (800) = -9.4 mg/cm²h
30	80 W% Coke Flour 20 W% 175°C Pitch 26 PPH B_4C 14 PPH Si	2500 PSI from R. T. to 2000°C 6250 PSI from 2000°C to 2650°C	B. D. = 2.14 g/cc ρ(25) W. G. = 4.2×10^{-4} OHM cm
31	80 W% Coke Flour 20 W% 175°C Pitch 5 PPH B_6Si	2500 PSI from R. T. to 2000°C 6250 PSI from 2000°C to 2600°C	B. D. = 2.07 g/cc S(25) W. G. = 8,300 PSI $\kappa\Big|_0^{30}$ (1200) = -280 mg/cm²h
32	80 W% Coke Flour 20 W% 175°C Pitch 7.5 PPH B_6Si	2500 PSI from R. T. to 2000°C 6250 PSI from 2000°C to 2600°C	B. D. = 2.12 g/cc $\kappa\Big|_0^{30}$ (1200) = -226 mg/cm²h
33	80 W% Coke Flour 20 W% 175°C Pitch 10 PPH B_6Si	2500 PSI from R. T. to 2000°C 6250 PSI from 2000°C to 2600°C	B. D. = 2.14 g/cc $\kappa\Big|_0^{30}$ (1200) = -158 mg/cm²h

Table 2, Continued

No.	Compositions	Processing Conditions Employed	Characteristics
34	80 W% Graphite Flour 20 W% 175°C Pitch 50 PPH TiB_2 18.5 PPH Si	2500 PSI from R. T. to 1800°C 4800 PSI at 1800°C	B. D. = 1.98 g/cc $\kappa \Big\vert_{0}^{180}$ (1200) = -6.1 mg/cm²h
35	80 W% Graphite Flour 20 W% 175°C Pitch 50 PPH TiB_2 9.25 PPH Si	2500 PSI from R. T. to 1800°C 4800 PSI at 1800°C	B. D. = 2.02 g/cc $\kappa \Big\vert_{0}^{x}$ (1200) see Fig. 19 $\kappa \Big\vert_{0}^{180}$ (1550) = -10.3 mg/cm²h
36	80 W% Graphite Flour 20 W% 175°C Pitch 82.5 PPH ZrB_2 18.5 PPH Si	2500 PSI from R. T. to 1800°C 4800 PSI at 1800°C	B. D. = 2.36 g/cc S(25) W. G. = 4,200 PSI $\kappa \Big\vert_{0}^{180}$ (1200) = -6.0 mg/cm²h
37	77.5 W% Graphite Flour 22.5 W% 175°C Pitch 82.5 PPH ZrB_2 18.5 PPH Si	2500 PSI from R. T. to 1800°C 6250 PSI from 1800°C to 2115°C	B. D. = 2.96 g/cc
38	73 W% Graphite Flour 27 W% 175°C Pitch 82.5 PPH ZrB_2 18.5 PPH Si GRADE JTA	2500 PSI from R. T. to 1800°C 6250 PSI from 1800°C to 2115°C	B. D. = 3.18 g/cc S(y) W. G. and A. G. see Fig. 25 λ (y) W. G. and A. G. see Fig. 26 ρ (y) W. G. and A. G. see Fig. 27 CTE(200) W. G. = 5.0 x 10^{-6}/°C CTE(200) A. G. = 6.4 x 10^{-6}/°C $\kappa \Big\vert_{0}^{x}$ (800, 1000, 1200, 1400) see Fig. 22 $\beta \Big\vert_{800}^{1685}$ see Fig. 33
39	73 W% Graphite Flour 27 W% 175°C Pitch 74.25 PPH ZrB_2 8.25 PPH B 18.5 PPH Si	2500 PSI from R. T. to 1800°C 6250 PSI from 1800°C to 2015°C	B. D. = 3.02 g/cc $\beta \Big\vert_{800}^{1685}$ see Fig. 34
40	73 W% Graphite Flour 27 W% 175°C Pitch 66 PPH ZrB_2 16.5 PPH B 18.5 PPH Si	2500 PSI from R. T. to 1800°C 6250 PSI from 1800°C to 1975°C	B. D. = 2.89 g/cc $\beta \Big\vert_{800}^{1685}$ see Fig. 34
41	73 W% Graphite Flour 27 W% 175°C Pitch 57.75 PPH ZrB_2 24.75 PPH B 18.5 PPH Si	2500 PSI from R. T. to 1800°C 6250 PSI from 1800°C to 1900°C	B. D. = 2.79 g/cc $\beta \Big\vert_{800}^{1685}$ see Fig. 34

Table 2, Continued

No.	Composition	Processing Conditions Employed	Characteristics
42	73 W% Graphite Flour 27 W% 175°C Pitch 66 PPH ZrB_2 8.25 PPH B 8.25 PPH Hf 18.5 PPH Si	2500 PSI from R.T. to 1800°C 6250 PSI from 1800°C to 1990°C	B.D. = 3.12 g/cc β 1685 / 800 see Fig. 35
43	73 W% Graphite Flour 27 W% 175°C Pitch 66 PPH ZrB_2 8.25 PPH B 8.25 PPH Cb 18.5 PPH Si	2500 PSI from R.T. to 1800°C 6250 PSI from 1800°C to 2010°C	B.D. = 3.06 g/cc β 1685 / 800 see Fig. 35
44	73 W% Graphite Flour 27 W% 175°C Pitch 66 PPH ZrB_2 8.25 PPH B 8.25 PPH TiB_2 18.5 PPH Si	2500 PSI from R.T. to 1800°C 6250 PSI from 1800°C to 1990°C	B.D. = 3.01 g/cc β 1685 / 800 see Fig. 35
45	73 W% Graphite Flour 27 W% 175°C Pitch 74.25 PPH ZrB_2 8.25 PPH TiB_2 18.5 PPH Si	2500 PSI from R.T. to 1800°C 6250 PSI from 1800°C to 2100°C	B.D. = 3.00 g/cc β 1685 / 800 = -0.043 mg/cm²°C
46	73 W% Graphite Flour 27 W% 175°C Pitch 74.25 PPH ZrB_2 8.25 PPH Hf 18.5 PPH Si	2500 PSI from R.T. to 1800°C 6250 PSI from 1800°C to 2235°C	B.D. = 3.09 g/cc β 1685 / 800 = -0.063 mg/cm²°C
47	73 W% Graphite Flour 27 W% 175°C Pitch 57.75 PPH ZrB_2 8.25 PPH B 16.5 PPH Cb 18.5 PPH Si	2500 PSI from R.T. to 1800°C 6250 PSI from 1800°C to 2115°C	B.D. = 3.10 g/cc β 1685 / 800 see Fig. 38
48	73 W% Graphite Flour 27 W% 175°C Pitch 49.5 PPH ZrB_2 8.25 PPH B 24.75 PPH Cb 18.5 PPH Si	2500 PSI from R.T. to 1800°C 6250 PSI from 1800°C to 2150°C	B.D. = 3.10 g/cc β 1685 / 800 see Fig. 38
49	73 W% Graphite Flour 27 W% 175°C Pitch 53.625 PPH ZrB_2 8.25 PPH B 20.625 PPH CrB_2 18.5 PPH Si	2500 PSI from R.T. to 1800°C 6250 PSI from 1800°C to 1980°C	B.D. = 2.90 g/cc β 1685 / 800 see Fig. 38

Table 2, Continued

No.	Composition	Processing Conditions Employed	Characteristics
50	73 W% Graphite Flour 27 W% 175°C Pitch 33 PPH ZrB_2 8.25 PPH B 41.25 PPH CrB_2 18.5 PPH Si	2500 PSI from R. T. to 1800°C 6250 PSI from 1800°C to 1900°C	B. D. = 2.76 g/cc β 1685 / 800 see Fig. 39
51	73 W% Graphite Flour 27 W% 175°C Pitch 66 PPH ZrB_2 8.25 PPH B 8.25 PPH Th 18.5 PPH Si	2500 PSI from R. T. to 1800°C 6250 PSI from 1800°C to 2120°C	B. D. = 2.71 g/cc β 1685 / 800 see Fig. 40
52	73 W% Graphite Flour 27 W% 175°C Pitch 49.5 PPH ZrB_2 8.25 PPH B 24.75 PPH Th 18.5 PPH Si	2500 PSI from R. T. to 1800°C 6250 PSI from 1800°C to 1960°C	B. D. = 2.86 g/cc β 1685 / 800 see Fig. 40
53	73 W% Graphite Flour 27 W% 175°C Pitch 33 PPH ZrB_2 8.25 PPH B 41.25 PPH Th 18.5 PPH Si	2500 PSI from R. T. to 1800°C 6250 PSI at 1800°C	B. D. = 3.16 g/cc β 1685 / 800 see Fig. 40
54	73 W% Graphite Flour 27 W% 175°C Pitch 66 PPH ZrB_2 8.25 PPH B 8.25 PPH Cb 9.25 PPH Th 9.25 PPH Si	2500 PSI from R. T. to 1800°C 6250 PSI from 1800°C to 2075°C	B. D. = 3.15 g/cc β 1685 / 800 see Fig. 41
55	73 W% Graphite Flour 27 W% 175°C Pitch 66 PPH ZrB_2 8.25 PPH B 8.25 PPH Cb 18.5 PPH Th	2500 PSI from R. T. to 1800°C 6250 PSI from 1800°C to 2120°C	B. D. = 3.08 g/cc β 1685 / 800 see Fig. 41
56	73 W% Graphite Flour 27 W% 175°C Pitch 66 PPH ZrB_2 8.25 PPH Cb 17.5 PPH B 9.25 PPH Si	2500 PSI from R. T. to 1800°C 6250 PSI from 1800°C to 2045°C	B. D. = 2.89 g/cc β 1685 / 800 see Fig. 42
57	73 W% Graphite Flour 27 W% 175°C Pitch 66 PPH ZrB_2 8.25 PPH Cb 26.75 PPH B	2500 PSI from R. T. to 1800°C 6250 PSI from 1800°C to 1965°C	B. D. = 2.92 g/cc β 1685 / 800 see Fig. 42 α 200 / 0 (800, 1100, 1400, 1600, 1660) see Table 1

7. OUTLOOK

Results of this study have shown that the achievement of permanent oxidation protection at elevated temperatures by means of composite technology is not only a promising principle but also a well-demonstrated reality. Methods of extending this principle to increasingly higher temperatures have been indicated and the following requirements evolve:

1) The protective coating formed by oxidation must not react with the base stock.

2) The reactions by which the coatings are formed must be accompanied by a volume increase of solid matter in order to provide self-sealing characteristics.

3) The coating must consist of one or more high-melting primary oxides bonded together by one or more auxiliary oxides. The latter may melt at relatively low temperatures, but must combine with the primary oxides to form solid solutions with high melting points.

4) The coating constituents must not evaporate to any significant extent under the conditions of intended applications.

5) The coatings should exhibit a certain degree of plasticity in the temperature range of application to absorb differences in thermal expansion between coating and base stock.

Not many systems can be expected to meet the given requirements and their selection is difficult since data on reaction kinetics, vaporization, plasticity, and mutual solid solubility of high-melting oxides are fairly rare. Nevertheless, the prospects are far from hopeless in that the results presented in this study were based on highly empirical approaches and can certainly not be considered the optimum achievement conceivable in this field. It is believed that with the help of supporting work on basic mechanisms, graphite base composites can be greatly improved over their present status and that it will be possible eventually to tailor them to given environmental requirements not satisfied by material presently available.

The relatively high cost of some of the composite ingredients make it desirable to form articles roughly to the final shape. To study such processing, a simple nose-cone shape was made by hot-pressing it from powder in very much the same manner as all the other composites

were manufactured. A cross section of the high temperature molding apparatus designed for this purpose is shown in Figure 44. The female die was made of a low porosity graphite, grade ZTE, which diminished losses of liquid phases from the composite during the pressing operation. Thermal expansion characteristics of the female die do not present any problems in this work since all composites of interest exhibit a larger CTE than normal graphites so that, on cooling after processing, the composite shrinks away from the female die. The situation is reversed with the male die and, therefore, this part was made of grade RVC, a nearly isotropic graphite with an exceptionally high CTE. This grade proved to be a satisfactory material for this application. No other problems were encountered. Figure 45 illustrates a successfully processed cone after removal from the mold.

Thus, the feasibility of producing preformed hardware from graphite base composites has been demonstrated, and it is hoped that this will eventually lead to practical applications.

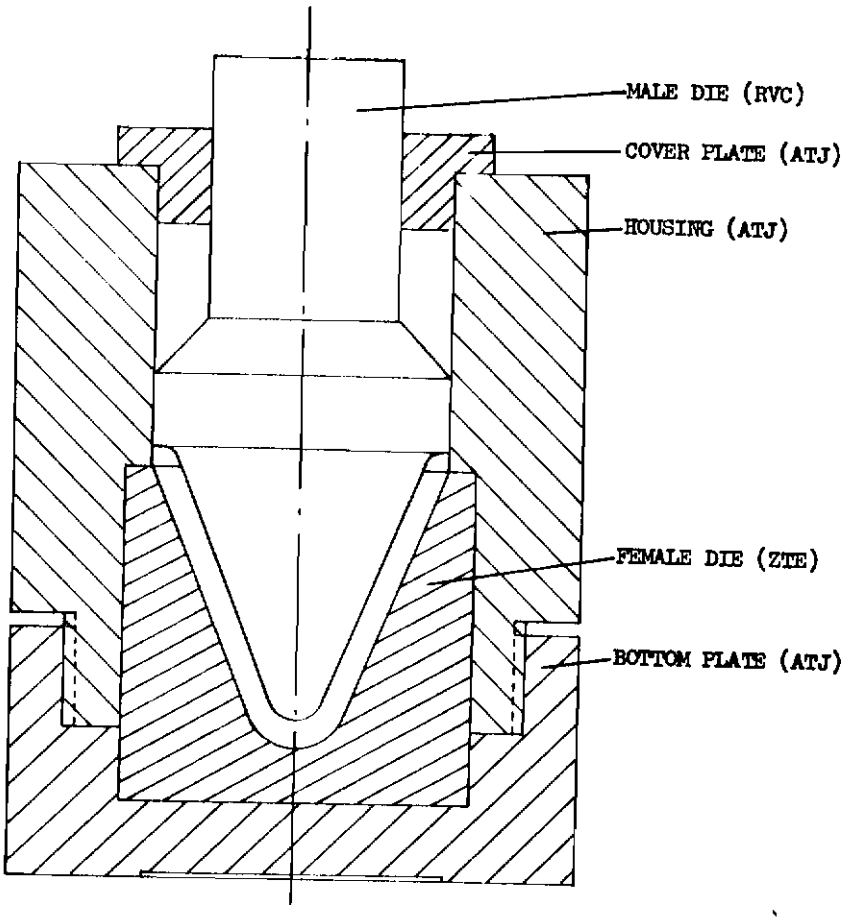

Figure 44. High Temperature Molding Apparatus for Nose Cone Fabrication, Cross Section

Figure 45. Nose Cone after Removal from the Mold

APPENDIX I. THEORY AND DESIGN OF LEVITATION EQUIPMENT FOR OXIDATION TEST

The following discussion gives some details of the theory and design of an apparatus to measure the oxidation resistance of a graphite specimen by levitating a test specimen through use of an electromagnetic field.

A spherical test specimen of graphite or graphite base composite is placed inside a coil which carries high frequency current. Repulsive forces appear between the current in the coil and eddy currents induced in the sphere. The intensity of these forces increases with increasing coil current and depends on the frequency used as well as on coil dimensions, sphere radius, and sphere resistivity.

Only centripetal forces are present when the centers of the sphere and coil coincide. If, starting from this position, the sphere is moved along the axis of the coil, a force component in the direction of this axis appears. In case of a vertical coil axis with the center of the sphere located above the center of the coil, the axial force component can be made to compensate for the weight of the sphere, thus causing levitation of the sphere.

The distance between the centers of the coil and sphere on the coil axis, called the "levitation height", determines the axial force in a characteristic fashion as shown schematically in Figure 46. The relationship between axial force and levitation height produces a pronounced

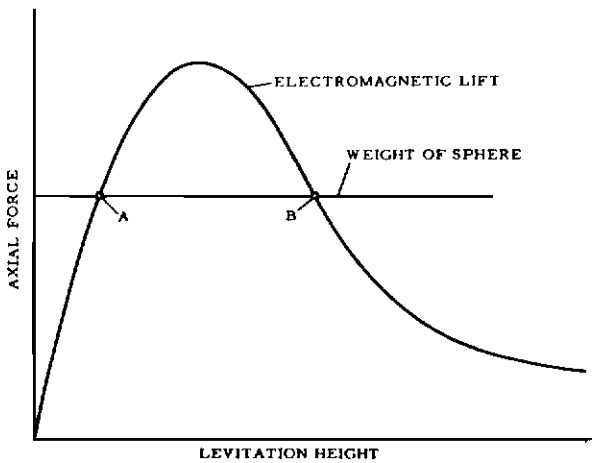

Figure 46. Levitation Characteristic, Axial Force versus Levitation Height

maximum and levitation is accomplished when the weight of the sphere is smaller than the force maximum. The weight line is seen to intersect the force curve in two points, A and B. A simple stability consideration shows that B is a stable point of equilibrium while A is not and, consequently, the sphere becomes suspended at the levitation height corresponding to point B. In this position, the current distribution in the sphere is not symmetrical with respect to a horizontal plane through the sphere center. High current densities will prevail in that region of the sphere which not only is close to the coil where the magnetic field is strong but also is characterized by reasonably large horizontal radii as counted from the vertical axis of the setup. The latter condition is due to the fact that the electric field strength and, in turn, the current density induced in horizontal circles around the vertical axis of the sphere, increases with increasing area of the circle since a larger circle encompasses a greater flux. This region of high current densities, called the "levitation belt", is shown schematically in Figure 47. The relative position of the levitation belt on the sphere shifts with changing levitation height as well as with changing coil diameter if the diameter of the sphere is kept constant. Significantly, a shift in position of the levitation belt changes the position of the point where the resultant of all electromagnetic forces acts on the sphere. This point, called the "center of electromagnetic buoyancy", necessarily coincides with the center of the sphere if the levitation height is zero; i. e., if the center of the sphere coincides with the center of the coil. On the other hand, when the center of the sphere is moved upwards along the vertical axis of the coil, the center of electromagnetic buoyancy will in general not coincide any more with the center of the sphere.

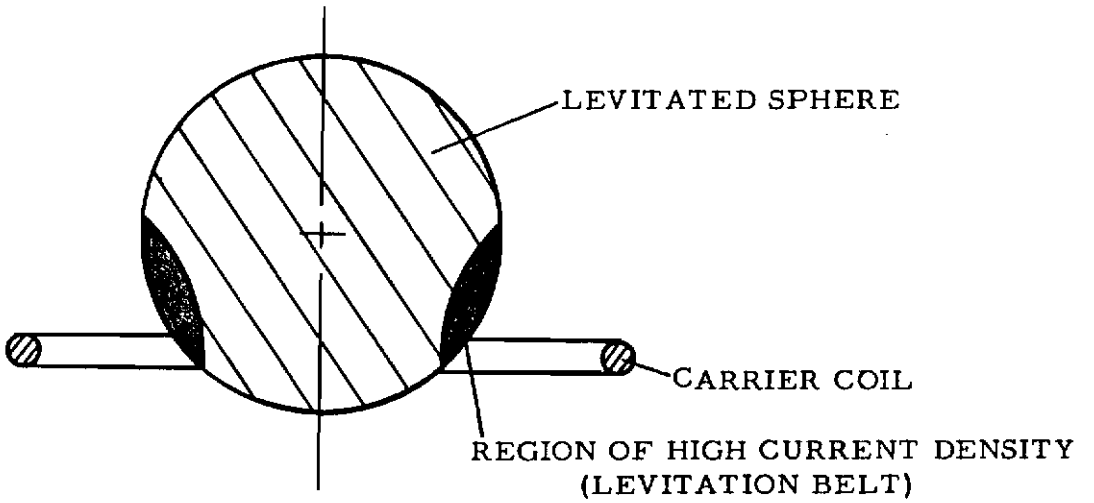

Figure 47. Levitated Sphere, Region of High Current Densities

This condition is used to produce rotational levitation which insures uniformity of temperature and oxidation in the given application. To explain the mechanics, it is interesting to compare the situation with that of a poorly designed boat, where a small rotation around the longitudinal axis can lead to capsizing when the center of buoyancy, generally below the center of mass, is shifted by this movement in such a way that a vertical plane through the new center of buoyancy intersects the vertical axis of the boat below the center of mass. The case of levitation, however, is quite different. Contrary to the boat situation, rotation of the sphere around a horizontal axis through the center of mass does not change the position of the center of electromagnetic buoyancy. Consequently, neither rotational oscillations nor "capsizing" can be incited in this fashion. Of further interest is a consideration of what happens when the equilibrium is disturbed by displacing the sphere in lateral (horizontal) direction. Evidently, such one-sided approach towards the carrier coil leads to a repulsive force driving the sphere back to the center. In general, as illustrated in Figure 48, this also creates a moment which turns the sphere. Nevertheless, this moment reverses as the sphere passes through its equilibrium position on the vertical axis of the coil towards the side opposite to the original displacement. While this explains the existence of lateral oscillations accompanied by "rolling" (rotational oscillations), it falls short of leading to conditions favoring continuous rotation. Such conditions were found to exist, however, when the carrier coil is not quite horizontal.

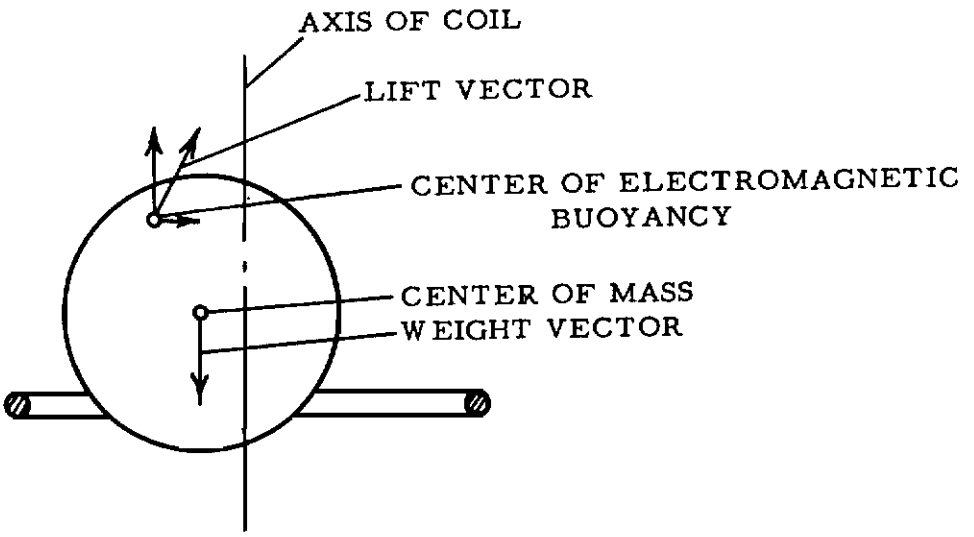

Figure 48. Levitated Sphere, Laterally Displaced

This is illustrated in Figure 49. If it is assumed that the sphere is released with its center on the axis of the coil, the electromagnetic lift force will fall into the coil axis. If it is assumed, furthermore,

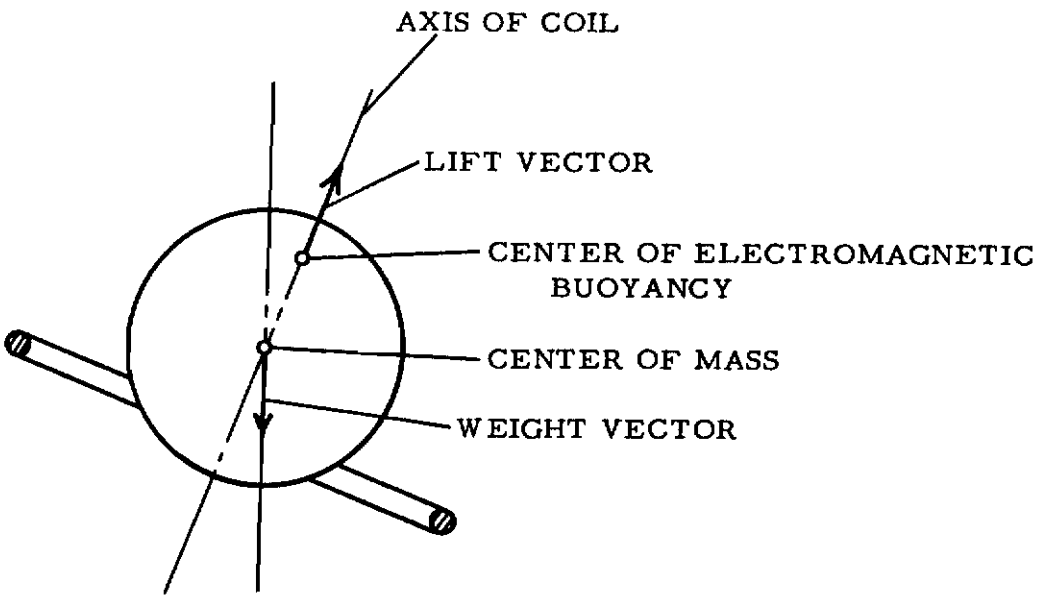

Figure 49. Levitated Sphere in Tilted Coil, Coaxial Position

that the vertical component of this force is equal to the weight of the sphere, equilibrium exists in the vertical but not in the horizontal direction. Consequently, the sphere will move towards the lower side of the inclined carrier coil. While this takes place, the center of electromagnetic buoyancy shifts, and the direction of the electromagnetic lift force changes in such a way that a component is created which pushes the sphere away from the coil side that it approaches; i. e., the electromagnetic lift force turns from its inclined direction towards the vertical. If, for the moment, inertia is neglected, equilibrium will be established when the electromagnetic lift force becomes vertical and equal to the sphere weight, the latter condition being self-adjusting by way of vertical movement. Due to its inertia, the sphere will overshoot its equilibrium position, but after several oscillations, its center of mass will come to

rest there. This condition is shown in Figure 50. While there is equilibrium of forces, a moment remains which turns the sphere around its center of mass, and it is immaterial for this effect whether the center of electromagnetic buoyancy was originally above or below the center of mass, the only difference being the direction of the resulting rotation.

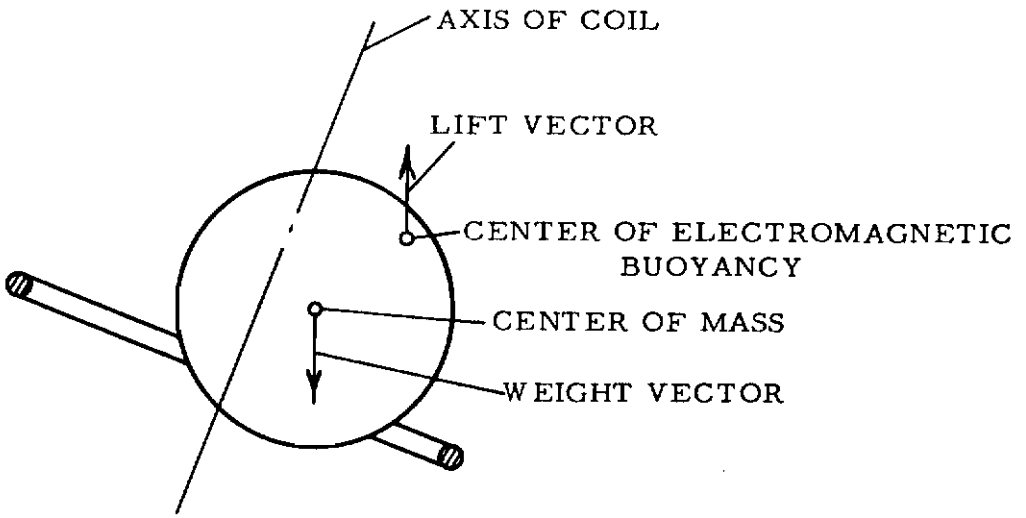

Figure 50. Levitated Sphere in Tilted Coil, Equilibrium Position

Further interesting aspects result from the fact that all composites prepared were necessarily anisotropic due to a pronounced orientation of the graphite particles during hot pressing. Even in fine flour, common graphite particles appear as needles or platelets. The given processing conditions cause them to align their maximum cross sections in planes perpendicular to the pressing direction. When a sphere of this anisotropy is levitated with the plane of the grain parallel to the plane of the coil, a state of metastability exists and the

smallest displacement from the equilibrium position leads to instability. The situation is illustrated in Figure 51. In this position, the given kind

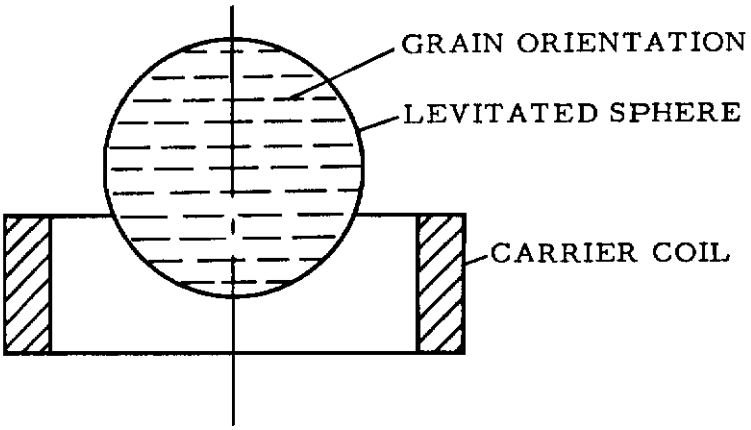

Figure 51. Levitated Sphere of Typical Anisotropy, Metastable Position

of sphere is comparable to a ring in that its "circumferential resistance" perpendicular to the coil is higher than the "circumferential resistance" in the plane of the coil. As illustrated in Figure 52, this results in a moment which turns the ring even further out of the original equilibrium position. Similarly, a sphere of the subject materials is turned until

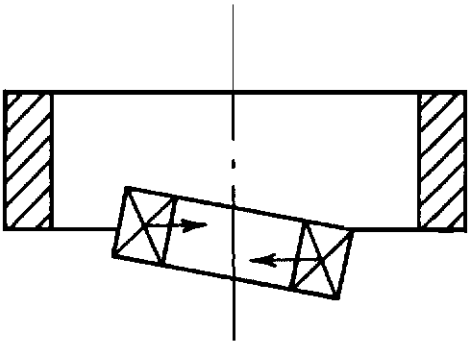

Figure 52. Levitated Ring, Unstable Position

it reaches the position indicated in Figure 53. In this state, excellent rotational stability prevails for the sphere with respect to a horizontal axis parallel to the planes of the grain. This, however, is not the case

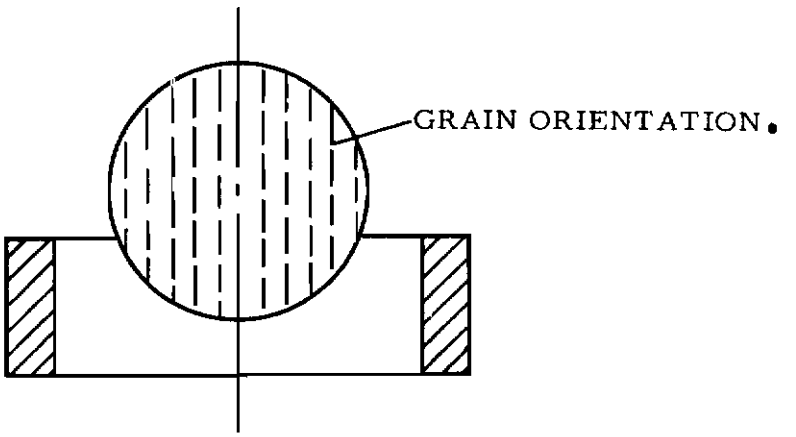

Figure 53. Levitated Sphere of Typical Anisotropy, Stable Position

for a horizontal axis perpendicular to the planes of the grain since all positions obtainable by turning the sphere around this axis are equivalent. The latter axis, called the "pole axis", is illustrated in Figure 54. According to the considerations presented above, smooth permanent rotation can be incited only if the pole axis is more or less perpendicular

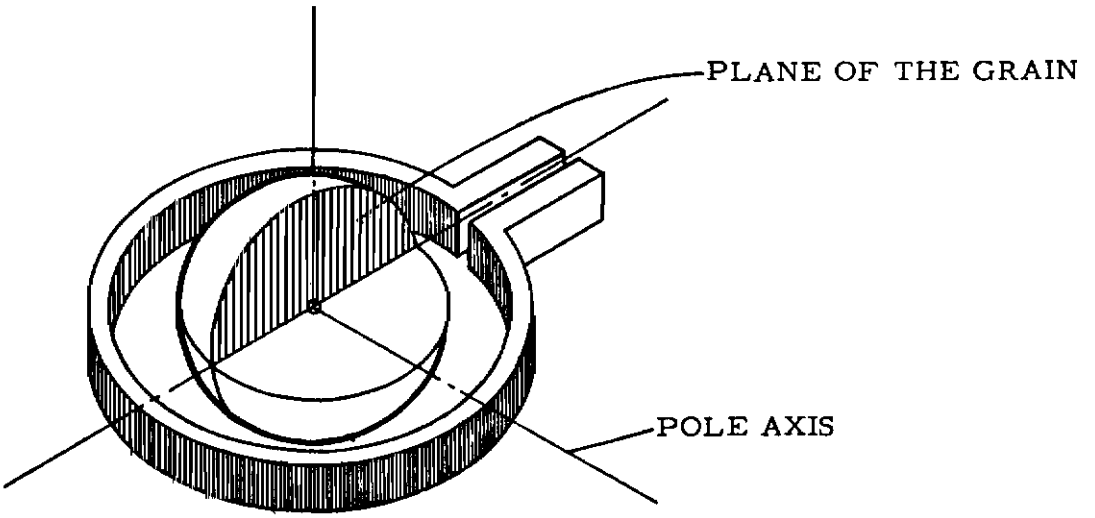

Figure 54. Pole Axis in Levitated Sphere of Typical Anisotropy

to the fall line of an inclined coil plane. Otherwise, the rotating moment has to overcome an electromagnetic countermoment. If it can do so, pulsating rotation results, and if it can not do so, only rotational oscillations occur and these eventually subside.

The levitation apparatus should be designed in such a way that the distance between the center of buoyancy and the center of mass is as great as possible to enforce rotation of the sphere. Although inclination of the carrier coil also promotes rotation of the sample, this method is quite limited because the sphere will jump over the lower side if the coil is tilted too far.

8. BIBLIOGRAPHY

Riley, M. W., "The New World of Carbon and Graphite". Materials in Design Engineering, September, 1962, pp. 113-128.

Zeitsch, K. J., "Oxidation Resistant Graphite Base Composites". Paper presented at the Sixth Meeting of the Refractory Composites Working Group, June 1962, Dayton, Ohio.

Zeitsch, K. J., "Oxidation Resistant Graphite Base Composites". U. S. Patent Application, Serial No. 203,691.